Received: 10 August 2022 | Revised: 19 February 2023 | Accepted: 22 February 2023

DOI: 10.1111/bph.16063

RESEARCH ARTICLE

# Veklury® (remdesivir) formulations inhibit initial membrane-coupled events of SARS-CoV-2 infection due to their sulfobutylether-β-cyclodextrin content

Tamas Kovacs | Kitti Kurtan | Zoltan Varga | Peter Nagy | Gyorgy Panyi | Florina Zakany

Department of Biophysics and Cell Biology, Faculty of Medicine, University of Debrecen, Debrecen, H-4032, Hungary

**Correspondence**
Florina Zakany, Department of Biophysics and Cell Biology, Faculty of Medicine, University of Debrecen, Egyetem tér 1, Debrecen H-4032, Hungary.
Email: florina.zakany@med.unideb.hu

**Funding information**
Hungarian National Research, Development and Innovation Office, Grant/Award Numbers: OTKA ANN133421, OTKA FK143400, OTKA K132906, OTKA K138075, OTKA K143071; Ministry of Innovation and Technology, Grant/Award Numbers: UNKP-21-4-II-DE-137, UNKP-21-4-II-DE-138; Ministry of Human Capacities, Hungary, Grant/Award Number: EFOP-3.6.2-16-2017-00006; Ministry of Finance, Hungary, Grant/Award Number: GINOP-2.3.2-15-2016-00015; Ministry of Culture and Innovation, Grant/Award Number: UNKP-22-4-II-DE-69

**Background and Purpose:** Despite its contradictory clinical performance, remdesivir (Veklury®) has a pivotal role in COVID-19 therapy. Possible contributions of the vehicle, sulfobutylether-β-cyclodextrin (SBECD) to Veklury® effects have been overlooked. The powder and solution formulations of Veklury® are treated equivalently despite their different vehicle content. Our objective was to study Veklury® effects on initial membrane-coupled events of SARS-CoV-2 infection focusing on the cholesterol depletion-mediated role of SBECD.

**Experimental Approach:** Using time-correlated flow cytometry and quantitative three-dimensional confocal microscopy, we studied early molecular events of SARS-CoV-2–host cell membrane interactions.

**Key Results:** Veklury® and different cholesterol-depleting cyclodextrins (CDs) reduced binding of the spike receptor-binding domain (RBD) to ACE2 and spike trimer internalization for Wuhan-Hu-1, Delta and Omicron variants. Correlations of these effects with cholesterol-dependent changes in membrane structure and decreased lipid raft-dependent ACE2–TMPRSS2 interaction establish that SBECD is not simply a vehicle but also an effector along with remdesivir due to its cholesterol-depleting potential. Veklury® solution inhibited RBD binding more efficiently due to its twice higher SBECD content. The CD-induced inhibitory effects were more prominent at lower RBD concentrations and in cells with lower endogenous ACE2 expression, indicating that the supportive CD actions can be even more pronounced during *in vivo* infection when viral load and ACE expression are typically low.

**Conclusion and Implications:** Our findings call for the differentiation of Veklury® formulations in meta-analyses of clinical trials, potentially revealing neglected benefits

**Abbreviations:** CD, cyclodextrin; CHOL, cholesterol complexed with MβCD; CTX-B, cholera toxin subunit B; Delta, B.1.617.2 variant strain of SARS-CoV-2; F66, *N*-[3-(40-dihexylamino-3-hydroxy-flavonyl-6-oxy)-propyl]*N*,*N*-dimethyl-*N*-(3-sulfopropyl)-ammonium inner salt; HPβCD, hydroxypropyl-β-cyclodextrin; MβCD, methyl-β-cyclodextrin; N*, normal excited state of F66; Omicron, B.1.1.529 Ba1 variant strain of SARS-CoV-2; RBD, receptor-binding domain; REM, remdesivir (GS-5734) in DMSO; SARS-CoV-2, severe acute respiratory syndrome coronavirus 2; SBECD, sulfobutylether-β-cyclodextrin; T*, tautomeric excited state of F66; Veklury® P, powder formulation of Veklury® (remdesivir), Veklury® S, solution formulation of Veklury® (remdesivir); WT, Wuhan-Hu-1 strain of SARS-CoV-2.

This is an open access article under the terms of the Creative Commons Attribution-NonCommercial-NoDerivs License, which permits use and distribution in any medium, provided the original work is properly cited, the use is non-commercial and no modifications or adaptations are made.
© 2023 The Authors. *British Journal of Pharmacology* published by John Wiley & Sons Ltd on behalf of British Pharmacological Society.

of the solution formulation, and also raise the possibility of adjuvant cyclodextrin (CD) therapy, even at higher doses, in COVID-19.

**KEYWORDS**
cholesterol, cyclodextrin, remdesivir, SARS-CoV-2, spike glycoprotein

## 1 | INTRODUCTION

Since its outbreak in 2019 in Wuhan, China, the coronavirus disease 2019 (COVID-19) pandemic remains the most serious health emergency situation nowadays (Zhu et al., 2020). Although different vaccines became available to reduce the incidence of life-threatening conditions, their effectiveness can be reduced against the continuously emerging severe acute respiratory syndrome coronavirus 2 (SARS-CoV-2) variants (Jackson et al., 2022; Tregoning et al., 2021; Willett et al., 2022) such as B.1.617.2 variant strain of SARS-CoV-2 (Delta) and B.1.1.529 Ba1 variant strain of SARS-CoV-2 (Omicron) carrying key mutations in the receptor-binding domain (RBD) of the **spike glycoprotein** (Meng et al., 2022; Planas et al., 2021). In parallel, efficient management of hospitalized severely diseased patients is still unresolved due to the lack of an available specific and powerful medication (Ho et al., 2022; Malek et al., 2021; Sanders et al., 2020). As a plausible first choice there is **remdesivir (Veklury®)**, a broad-spectrum adenosine-analogue prodrug that inhibits the structurally conserved viral RNA polymerases (Cho et al., 2012; Warren et al., 2016), a repurposed medication which, initially, was described as effective against Ebola virus (Siegel et al., 2017; Warren et al., 2016) and, subsequently, severe acute respiratory syndrome coronavirus 1 (SARS-CoV-1) and Middle East respiratory syndrome coronavirus (MERS-CoV) (de Wit et al., 2020; Sheahan et al., 2017, 2020). Due to its ability to inhibit SARS-CoV-2 replication, which reduces infection *in vitro* and *in vivo* (Choy et al., 2020; Pruijssers et al., 2020; Wang et al., 2020; Williamson, Feldmann, et al., 2020), it reduces recovery time, improves clinical status and decreases mortality in hospitalized patients, as reported in early clinical studies (Beigel et al., 2020; Spinner et al., 2020). Thus remdesivir became the first antiviral drug approved by the US Food and Drug Administration and the European Medicines Agency for the treatment of COVID-19 under the trade name Veklury® from Gilead Sciences. Subsequent randomized controlled trials overshadowed early optimism towards remdesivir treatment because its application was not linked to significant clinical benefits (Ader et al., 2022; Kaka et al., 2022; World Health Organization [WHO] Solidarity Trial Consortium, 2021). Nevertheless, the National Institutes of Health (NIH) guideline proposes remdesivir as a basic drug in the therapeutic regime for COVID-19 with special indications, supporting its worldwide medical application (COVID-19 Treatment Guidelines Panel of NIH, 2022). Furthermore, a recent trial demonstrated that early remdesivir could prevent progression of the disease to the severe form in outpatients (Gottlieb et al., 2022).

### What is already known

- Veklury® (remdesivir), formulated as powder or solution, is a well-established drug in COVID-19 therapy.
- The contribution of the vehicle, sulfobutylether-β-cyclodextrin (SBECD) to the therapeutic effect has not been investigated.

### What does this study add

- Cholesterol-depleting cyclodextrins and Veklury® (remdesivir) formulations, due to their SBECD content, disrupt lipid rafts.
- This effect is accompanied by the inhibition of ACE2 binding and internalization of SARS-CoV-2 spike glycoprotein.

### What is the clinical significance

- The findings suggest that Veklury® solution should be preferred due to its higher SBECD content.
- The results propose that well-tolerable cyclodextrins could be efficiently used as adjuvants in COVID-19.

The initial cellular events of SARS-CoV-2 infection primarily involve interactions with the host cell membrane and are highly influenced by its **cholesterol** content (Li et al., 2021; Palacios-Rápalo et al., 2021; Wang et al., 2021). Cholesterol-enriched lipid rafts organize viral entry points by ensuring the vicinity between **angiotensin-converting enzyme 2 (ACE2)**, the receptor for the viral spike glycoproteins, and **transmembrane serine protease 2 (TMPRSS2)**, the main cell surface protease responsible for spike processing leading to membrane fusion and concomitant cytoplasmic uptake of viral RNA (Hoffmann et al., 2020; Jackson et al., 2022; Palacios-Rápalo et al., 2021; Zhou et al., 2020). In certain cell types with low TMPRSS2 expression, lipid raft-mediated or clathrin-dependent endocytic pathways, also depending on cholesterol, target viral particles to endosomal compartments leading to cathepsin-mediated cleavage of spike proteins and subsequent cytoplasmic entry (Bayati et al., 2021;

14765381, 0, Downloaded from https://bpspubs.onlinelibrary.wiley.com/doi/10.1111/bph.16063 by Cochrane Hungary, Wiley Online Library on [03/04/2023]. See the Terms and Conditions (https://onlinelibrary.wiley.com/terms-and-conditions) on Wiley Online Library for rules of use; OA articles are governed by the applicable Creative Commons License

Hoffmann et al., 2020; Jackson et al., 2022; Li et al., 2021; Ou et al., 2020; Ripa et al., 2021). In spite of the original Wuhan-Hu-1 strain (wild-type [WT]) and the Delta variant mainly relying on the TMPRSS2-mediated route, the recently emerged Omicron Ba1 variant preferentially uses endocytosis- and cathepsin-based entry (Meng et al., 2022; Willett et al., 2022). The pathways used by all variants substantially depend on cholesterol. Consistently, obesity and cholesterol-related cardiovascular diseases are well-known risk factors for increased disease severity (Guo et al., 2020; Williamson et al., 2020). Veklury® is available as a powder (Veklury® P) or as a concentrated solution (Veklury® S), both containing sulfobutylether-β-cyclodextrin (SBECD) as the vehicle to increase solubility of the otherwise poorly water-soluble remdesivir (Szente et al., 2021). Although the two formulations have a major difference in the relative amount of SBECD (3 g in powder compared with 6 g in solution of a single dose of 100-mg remdesivir given by intravenous infusion [Gilead Sciences, Inc., 2022]), they are considered equivalent in clinical practice (COVID-19 Treatment Guidelines Panel of NIH, 2022; WHO, 2022). While all the experimental and clinical studies examining the effectiveness of Veklury® focused solely on remdesivir as the 'active' component, a possible contribution of the 'inert carrier' to the effects through membrane cholesterol depletion and concomitant interference with initial cellular steps of viral infection were not evaluated despite the relatively high and different SBECD content in the formulations. Furthermore, although numerous studies hypothesized the potential beneficial effects of cyclodextrins (CDs) in COVID-19 (Fecchi et al., 2020; Garrido et al., 2020; Palacios-Rápalo et al., 2021; Sorice et al., 2020; Zakany et al., 2022), these have not been confirmed experimentally using Veklury® formulations or CDs applied in medical practice.

The objective of the current study was to examine whether cholesterol-dependent early membrane-coupled cellular steps of SARS-CoV-2 infection can be affected by Veklury® (remdesivir) formulations due to their SBECD content independent of remdesivir. Using time-correlated flow cytometry and three-dimensional (3D) analysis of confocal microscopic images, we tested whether Veklury® P, Veklury® S, SBECD or remdesivir alone influenced: (i) binding of spike RBD to ACE2, (ii) colocalization of ACE2, TMPRSS2 and lipid rafts, and (iii) cellular uptake of SARS-CoV-2 spike trimers for both the Wuhan-Hu-1 strain (WT) and Delta variants. To support the SBECD-mediated cholesterol extraction-based action of Veklury® we also applied hydroxypropyl-β-cyclodextrin (HPβCD), a CD with an established clinical application, to reduce cellular cholesterol in Niemann–Pick disease, methyl-β-cyclodextrin (MβCD), the most efficient cholesterol-complexing CD *in vitro*, and cholesterol loading. We also tested if Veklury® S, containing twice higher amount of SBECD than Veklury® P, inhibits RBD binding more efficiently than Veklury® P at identical remdesivir concentrations, and whether supplementation of Veklury® P with SBECD can mirror the increased potency of Veklury® S. We compared the effects of these treatments in Calu-3, a cell line with an endogenous, low expression of ACE2, and an ACE2- and TMPRSS2-overexpressing HEK cell line, and at low RBD concentrations mimicking physiological conditions to emphasize the biological relevance of our results. To underline the potential applicability of our findings to the continuously appearing novel SARS-CoV-2 variants with still cholesterol-dependent cellular entry, we further examined Veklury® P, Veklury® S and SBECD actions on the Omicron Ba1 variant as well.

## 2 | METHODS

### 2.1 | Cell cultures and treatments

The human embryonic kidney HEK293T cell line stably expressing ACE2 and TMPRSS2 genes (HEK/ACE2 + TMPRSS2) was obtained from GeneCopoeia (Rockville, MD; SL222), whereas the Calu-3 lung adenocarcinoma cell line with endogenous expression of ACE2 and TMPRSS2 was from the American Type Culture Collection (Manassas, VA; HTB-55). Both cell lines were cultivated according to their specifications.

In our experiments, HEK/ACE2 + TMPRSS2 or Calu-3 cells were treated with various test compounds (see below) dissolved in normal Ringer's solution (in mM: 145 NaCl, 5 KCl, 10 HEPES, 5.5 glucose, 2.5 $CaCl_2$ and 1 $MgCl_2$, pH 7.35) for 1 h followed by extensive washing before further investigation.

### 2.2 | Examination of lipid raft integrity using confocal laser-scanning microscopy

HEK/ACE2 + TMPRSS2 cells grown on eight-well chambered coverslip (ibidi, Gräfelfing, Germany; 80826) were treated for 1 h at room temperature with MβCD, HPβCD, SBECD, Veklury® P or Veklury® S at CD concentrations of 1, 5 and 10 mM, with cholesterol complexed with MβCD (CHOL) at 200 μM or pure remdesivir (GS-5374; REM) at 100 μM. After washing, the samples were labelled with 10-nM *N*-[3-(40-dihexylamino-3-hydroxy-flavonyl-6-oxy)-propyl]*N*,*N*-dimethyl-*N*-(3-sulfopropyl)-ammonium inner salt (F66) and 8-μg·ml$^{-1}$ Alexa Fluor 647-conjugated cholera toxin subunit B (CTX-B) for 20 min on ice. Images were acquired from the flat, bottom membrane region of the cells adjacent to the coverslip using an LSM880 confocal laser-scanning microscope (Carl Zeiss AG, Jena, Germany). Alexa Fluor 647 was excited at 633 nm and its emission was detected between 649 and 759 nm, whereas F66 was examined with an emission radiometric assay shown to be responsive to changes in the dipole potential (Kovacs et al., 2017; Zakany et al., 2021). The dye was excited at 405 nm and its emission was measured in two different wavelength ranges, 463–527 and 543–589 nm, corresponding to the normal (N*) and tautomeric (T*) forms of its excited state, respectively. Image processing was carried out in manually selected pixels corresponding to the cell membrane with the DIPimage toolbox (Delft University of Technology, Delft, the Netherlands) under MATLAB (MathWorks, Natick, MA) as described previously (Kovacs et al., 2017). Briefly, during image analysis, segmentation of images was performed with a custom-written

14765381, 0, Downloaded from https://bpspubs.onlinelibrary.wiley.com/doi/10.1111/bph.16063 by Cochrane Hungary, Wiley Online Library on [03/04/2023]. See the Terms and Conditions (https://onlinelibrary.wiley.com/terms-and-conditions) on Wiley Online Library for rules of use; OA articles are governed by the applicable Creative Commons License

algorithm in which a threshold intensity was determined for CTX-B using the maxentropy algorithm confirmed by visual inspection. Membrane pixels were considered 'raft' or 'non-raft' pixels if their intensity was above or below the determined threshold, respectively. Average T*/N* fluorescence intensity ratios positively correlating with the magnitude of dipole potential were separately calculated from individual pixels in the CTX-B high 'raft' and CTX-B low 'non-raft' regions after background subtraction. Alternatively, because the magnitude of dipole potential is significantly higher in lipid rafts (Kovacs et al., 2017), a threshold value of the intensity ratio was determined after comparison of pixelwise intensity ratio histograms of CTX-B high and CTX-B low regions, and 'raft' and 'non-raft' pixels were defined as having larger or smaller T*/N* ratio values, respectively, when compared to the threshold. This was followed by calculation of the area fraction of 'raft' pixels in each cell compared to all membrane pixels.

## 2.3 | Investigation of SARS-CoV-2 spike RBD binding to ACE2 using flow cytometry

For the investigation of the time dependence of WT and Delta SARS-CoV-2 spike RBD binding to cell surface ACE2, HEK/ACE2 + TMPRSS2 cells were trypsinized and treated for 1 h at room temperature with MβCD at various concentrations ranging from 0.25 to 10 mM. After washing, the cellular binding of GFP (green fluorescent protein)-tagged WT (GenBank: MN908947.3) and Delta (B.1.617.2, Indian variant) SARS-CoV-2 spike RBD (trenzyme, Konstanz, Germany; P2020-031 and P2020-049, respectively) was quantified with a NovoCyte 3000RYB flow cytometer (ACEA Biosciences, San Diego, CA). GFP was excited at 488 nm, and the emitted intensity was detected using a 530/30 emission filter. Measurements started immediately after addition of RBD and continued for 5 min. Experimental data were analysed first in FCS Express (De Novo Software, Los Angeles, CA). Time-correlated fluorescence intensity values of cells with a normal morphology on forward scatter (FSC)–side scatter (SSC) dot plots were exported, and the moving averages of samples were calculated with a window size of 10 s using a custom-written MATLAB algorithm (Batta et al., 2021). During analysis, fluorescence intensity values determined in the given time windows were normalized to the average of intensities determined in the last time window of untreated control samples. Experiments were carried out at different RBD concentrations ranging between 0.05 and 5 μg·ml$^{-1}$.

Alternatively, HEK/ACE2 + TMPRSS2 and Calu-3 cells were trypsinized and treated for 1 h at room temperature with MβCD, HPβCD, SBECD, Veklury® P, Veklury® S or 1:1 (w/w) Veklury® P: SBECD solutions at CD concentrations ranging between 0.078 and 20 mM, with CHOL between 12.5 and 800 μM or REM between 75 and 1200 μM. After washing, HEK/ACE2 + TMPRSS2 cells were incubated in the presence of 0.2-μg·ml$^{-1}$ WT or 0.1-μg·ml$^{-1}$ Delta RBD–GFP, whereas Calu-3 cells were labelled with 1-μg·ml$^{-1}$ WT or 0.5-μg·ml$^{-1}$ Delta RBD–GFP for 4 min followed by measurement of GFP fluorescence intensities in a time window of 30 s. For investigating the Omicron variant (Omicron B.1.1.529 Ba1), experiments were repeated after SBECD, Veklury® P or Veklury® S treatments at CD concentrations of 1, 5 and 10 mM in HEK/ACE2 + TMPRSS2 and Calu-3 cells using Omicron RBD–GFP (trenzyme; P2020-061) at 0.2 and 1 μg·ml$^{-1}$, respectively. During data analysis in FCS Express, average intensity values were calculated in each sample from data of cells with a normal morphology on FSC–SSC dot plots and subsequently normalized to the mean value determined in untreated control samples.

## 2.4 | Determination of cell surface ACE2 expression using flow cytometry

HEK/ACE2 + TMPRSS2 and Calu-3 cells were trypsinized and treated for 1 h at room temperature with MβCD, HPβCD, SBECD, Veklury® P or Veklury® S at CD concentrations of 1, 5 and 10 mM, with CHOL at 200 μM or REM at 100 μM. After washing, HEK/ACE2 + TMPRSS2 cells were incubated for 30 min in the presence of Alexa Fluor 488-tagged anti-ACE2 antibody (R&D Systems; FAB9332G) applied at a dilution of 1:50. Fluorescence intensities of individual cells were measured with a NovoCyte 3000RYB flow cytometer. Alexa Fluor 488 was excited at 488 nm, and the emitted intensity was detected using a 530/30 emission filter. During data analysis in FCS Express, average intensity values were calculated in each sample from data of cells with a normal morphology on FSC–SSC dot plots and subsequently normalized to the mean value determined in untreated control samples.

## 2.5 | Analysis of the colocalization between lipid rafts, ACE2 and TMPRSS2 using confocal laser-scanning microscopy

HEK/ACE2 + TMPRSS2 cells grown on eight-well chambered coverslip were treated for 1 h at room temperature with MβCD, HPβCD, SBECD, Veklury® P or Veklury® S at CD concentrations of 1, 5 and 10 mM, with CHOL at 200 μM or REM at 100 μM. After washing, cells were subsequently labelled with 8-μg·ml$^{-1}$ Alexa Fluor 647-conjugated CTX-B and Alexa Fluor 488-tagged anti-ACE2 antibody applied at a dilution of 1:50. Alternatively, cells were labelled with 8-μg·ml$^{-1}$ Alexa Fluor 488-conjugated CTX-B (Thermo Fisher; C22841) and anti-TMPRSS2 antibody (Thermo Fisher; PA5-14265) applied at a dilution of 1:50, which was visualized with secondary labelling using Alexa Fluor 647-tagged goat anti-rabbit IgG (Thermo Fisher; A-21245) at a dilution of 1:500. In the third part of these measurements, cells were labelled with Alexa Fluor 488-tagged anti-ACE2 and anti-TMPRSS2 antibodies, followed by secondary staining of the latter antibody with Alexa Fluor 647-tagged goat anti-rabbit IgG. The Alexa Fluor 488-tagged anti-ACE2 antibody was of mouse origin preventing cross-reaction of the secondary antibody. Images were taken from the flat, bottom membrane of cells adjacent to the coverslip using a Zeiss LSM880 confocal laser-scanning microscope. Alexa Fluor

14765381, 0, Downloaded from https://bpspubs.onlinelibrary.wiley.com/doi/10.1111/bph.16063 by Cochrane Hungary, Wiley Online Library on [03/04/2023]. See the Terms and Conditions (https://onlinelibrary.wiley.com/terms-and-conditions) on Wiley Online Library for rules of use; OA articles are governed by the applicable Creative Commons License

488 and Alexa Fluor 647 were excited at 488 and 633 nm, respectively, and their emission was detected in the wavelength ranges of 493–540 and 650–755 nm, respectively. During image processing after manual selection of membrane pixels, the Pearson correlation coefficient between fluorescence intensities of the two applied fluorophores was determined from pixelwise data of individual cells using a custom-written algorithm under MATLAB. To rule out the accidental positive correlation, we determined the 95% confidence interval of the coefficient assuming no correlation between the analysed parameters for each image according to the method of Costes as previously (Kovacs et al., 2017).

## 2.6 | Examination of SARS-CoV-2 spike trimer internalization using confocal laser-scanning microscopy

HEK/ACE2 + TMPRSS2 and Calu-3 cells grown on eight-well chambered coverslip were treated for 1 h with MβCD, HPβCD, SBECD, Veklury® P or Veklury® S at CD concentrations of 1 and 5 mM, with CHOL at 200 μM or REM at 100 μM. After washing, HEK/ACE2 + TMPRSS2 cells were subsequently incubated for 4 h at 37°C in the presence of 0.5-μg·ml$^{-1}$ WT or 0.25-μg·ml$^{-1}$ Delta spike trimer conjugated with Alexa Fluor 488 (R&D Systems; AFG10561 and AFG10878, respectively), whereas Calu-3 cells were labelled with 2.5-μg·ml$^{-1}$ WT or 1.25-μg·ml$^{-1}$ Delta trimer tagged with Alexa Fluor 488. When using Omicron spike trimer conjugated with Alexa Fluor 488 (R&D Systems; AFG11060), experiments were repeated after SBECD, Veklury® P or Veklury® S treatments in HEK/ACE2 + TMPRSS2 and Calu-3 cells using the trimer at 0.5 and 2.5 μg·ml$^{-1}$, respectively. These trimer concentrations were identical in molar concentrations to those used in RBD binding experiments. In the last 15 min, cells were stained with 10-nM F66 to visualize cell membranes. After washing, 15–20 confocal slices were acquired from the cells with a Zeiss LSM880 confocal laser-scanning microscope. F66 and Alexa Fluor 488 were excited at 405 and 488 nm, respectively, whereas their emitted intensities were detected in wavelength ranges of 440–480 and 493–550 nm, respectively. During image analysis, pixels corresponding to the plasma membrane and the intracellular space were identified in F66 Z-stack images using a custom-written 3D watershed algorithm in MATLAB, and the average fluorescence intensity values emitted by Alexa Fluor 488 were calculated using data of intracellular pixels for each cell. The obtained values were normalized to the median value determined from data of individual cells in untreated control samples.

## 2.7 | Testing cell viability using flow cytometry

HEK/ACE2 + TMPRSS2 and Calu-3 cells were trypsinized and treated for 1 h at room temperature with HPβCD, SBECD, Veklury® P or Veklury® S at CD concentrations of 5, 10 and 20 mM, or, as a positive control, 0.5% Triton X-100 (Sigma-Aldrich, St. Louis, MO; X100). After washing, cells were labelled with SYTOX Green Dead Cell Stain and Alexa Fluor 647-conjugated Annexin V at dilutions of 1:1000 and 1:20, respectively, in Annexin binding buffer for 15 min at room temperature. Fluorescence intensities of individual cells were subsequently measured using a NovoCyte 3000RYB flow cytometer. SYTOX Green and Alexa Fluor 647 fluorophores were excited at 488 and 640 nm, respectively, and emitted intensities were measured using 530/30 and 660/20 emission filters, respectively. During data analysis, the fractions of SYTOX Green and Annexin V negative living cells were calculated for each sample using FCS Express and subsequently normalized to the mean value determined in untreated control samples.

## 2.8 | Data handling and statistical analysis

Experiments were performed in a blinded way because the treatments and measurements were carried out by different persons and the latter was unaware of the type of treatment for the given samples. Furthermore, primary analysis of experimental data was also blinded because analyses and the experiments were performed by different persons and the analyser was unaware of the experimental conditions. Randomization is irrelevant in the case of this study because all compared samples originated from the same culture flask. However, treatments and measurements were carried out in different order to eliminate differences due to timing of experiments.

Measured data are generally represented as mean ± SD from n number of cells from at least five different experiments for confocal microscopy or n number of independent experiments containing data of at least 10,000 (time-point measurements) or 50,000 (kinetic measurements) cells of normal morphology per sample for flow cytometry. In the experiment investigating spike trimer uptake, median and first and third quartile values are plotted. For the microscopic and cytometric measurements, we tried to ensure that the sample sizes were approximately the same; however, the experimental conditions (slightly different number of cells of normal morphology after washing steps in flow cytometry, slightly different number of cells in a single field of view in microscopic images or imperfect identification of all cells in confocal images by the image-segmenting watershed algorithm) did not allow exactly matching sample sizes. Group size selection for each experimental protocol was based on power analysis using type I and type II error probabilities of 0.05 and 0.2, respectively. For flow cytometry, an expected change with the magnitude of two SDs predicted that a sample size of $n \geq 5$ would be required for firm statistical significance. However, for microscopic analysis, due to altered SDs originating from single cell analysis, we carried out power analysis applying expected changes of one SD for lipid raft disruption and colocalization experiments, whereas one-third SD was used for trimer uptake analysis, which gave required sample sizes of $n \geq 17$ and $n \geq 150$, respectively. The

14765381, 0, Downloaded from https://bpspubs.onlinelibrary.wiley.com/doi/10.1111/bph.16063 by Cochrane Hungary, Wiley Online Library on [03/04/2023]. See the Terms and Conditions (https://onlinelibrary.wiley.com/terms-and-conditions) on Wiley Online Library for rules of use; OA articles are governed by the applicable Creative Commons License

declared group sizes represent the numbers of independent values, and statistical analysis was done using these independent values. Flow cytometry and trimer uptake data were normalized to the mean and median, respectively, of untreated control samples, which was required to reduce within-group variability due to differences between initial fluorescence intensities, which would have obscured between-group differences. Outliers were included in data analysis and presentation. Statistical analysis was carried out in GraphPad Prism (La Jolla, CA). Statistical analysis was undertaken only for studies where each group size was at least $n = 5$. Multiple comparisons were performed with one- or two-way ANOVA, and $P$ values were calculated based on post hoc Tukey's HSD tests that were conducted only if the data were normally distributed and F in ANOVA achieved $P < 0.05$. All differences were considered statistically significant when $P < 0.05$. Exact values of the parameters calculated during statistical analysis are summarized in supporting information tables for each figure. The data and statistical analysis comply with the recommendations of the British Journal of Pharmacology on experimental design and analysis in pharmacology (Curtis et al., 2022).

## 2.9 | Materials

Methyl-β-cyclodextrin (MβCD; CYL-1859), hydroxypropyl-β-cyclodextrin (HPβCD; CYL-4259), sulfobutylether-β-cyclodextrin (SBECD; CYL-4815) and cholesterol complexed with MβCD (CHOL, CYL-3644) were obtained from CycloLab Cyclodextrin R&D Laboratory (Budapest, Hungary). Veklury® in both powder (Veklury® P) and solution (Veklury® S) forms were produced by Gilead Sciences (Foster City, CA). Pure remdesivir (REM, GS-5734) was from R&D Systems (Minneapolis, MN; 7226) and dissolved in DMSO with the DMSO concentration being always lower than 0.05% during treatments of cells. *N*-[3-(40-dihexylamino-3-hydroxy-flavonyl-6-oxy)-propyl]*N*,*N*-dimethyl-*N*-(3-sulfopropyl)-ammonium inner salt (F66) was a kind gift from Andrey Klymchenko (Université de Strasbourg, Strasbourg, France). Cholera toxin subunit B (CTX-B; C34778), SYTOX Green Dead Cell Stain (S7020) and Alexa Fluor 647-conjugated Annexin V (A23204) were purchased from Thermo Fisher, Waltham, MA, U.S.A. Triton X-100 was obtained from Sigma-Aldrich, St. Louis, MO, U.S.A.; X100. Details of other materials and suppliers were provided in the specific sections.

## 2.10 | Nomenclature of targets and ligands

Key protein targets and ligands in this article are hyperlinked to corresponding entries in the IUPHAR/BPS Guide to PHARMACOLOGY http://www.guidetopharmacology.org and are permanently archived in the Concise Guide to PHARMACOLOGY 2021/22 (Alexander, Fabbro, et al., 2021, Alexander, Kelly, et al., 2021).

# 3 | RESULTS

## 3.1 | Changes in cell membrane structure induced by Veklury® (remdesivir) formulations and cyclodextrins (CDs) lead to disruption of lipid rafts and are correlated with membrane cholesterol

CDs can extract membrane cholesterol and consequently alter biophysical properties of the cell membrane and disrupt raft microdomains (Kovacs et al., 2021, 2022; Zidovetzki & Levitan, 2007). Due to the SBECD content of Veklury® formulations, they may also induce alterations in the organization of the cell membrane (Davidson et al., 2016). However, this has not been tested yet. To establish that the CD component of Veklury® formulations may be of medical relevance, we assessed the ability of Veklury® P, Veklury® S, their vehicle SBECD and the 'active' component REM, applied in concentrations approximating to the therapeutic dose (see Section 4), to modify membrane structure and induce lipid raft disruption in HEK/ACE2 + TMPRSS2 cells. In addition, we compared the effects of these compounds with those of HPβCD, another cholesterol-complexing CD used *in vivo* (Loftsson & Brewster, 2010; Stella & He, 2008; Zakany et al., 2022), and MβCD, the CD derivative with the highest *in vitro* cholesterol-binding efficiency (Kovacs et al., 2021; Szente et al., 2018), to test the maximal potential extents of CD-induced effects. To support the correlation between the observed CD-induced alterations of membrane structure and membrane cholesterol levels, we also examined changes in response to cholesterol supplementation using cholesterol–MβCD complexes (CHOL). We employed a confocal microscopy-based emission radiometric approach to quantify alterations in membrane biophysical properties in living cells utilizing F66, an environment-sensitive fluorophore with two well-separated bands in its emission spectrum corresponding to normal (N*) and tautomer (T*) excited states. The T*/N* emission ratio of F66 positively correlates with the magnitude of dipole potential, a membrane biophysical parameter strongly related to membrane hydration and fluidity and substantially determined by membrane cholesterol level with having larger emission ratio in lipid rafts when compared to non-raft regions (Kovacs et al., 2017; Zakany et al., 2021). We labelled HEK/ACE2 + TMPRSS2 cells with F66 and CTX-B, a widely applied marker of lipid rafts due to its selective binding to raft-resident GM1 ganglioside (Kovacs et al., 2017). Images were recorded from the flat, bottom membrane region of cells adjacent to the coverslip (Figure 1a) and the F66 T*/N* fluorescence ratio was determined on a pixel-by-pixel basis, whereas the CTX-B images were segmented into raft and non-raft regions based on CTX-B intensities. Consistent with our previous results (Kovacs et al., 2017), we observed that the F66 T*/N* ratio was larger in CTX-B high raft regions than in CTX-B low non-raft membrane pixels (Figure 1b). Similarly, the average F66 T*/N* ratios were systematically higher in CTX-B high raft domains than outside them in all treated samples (Figure 1c filled circles vs. empty squares and Table S1). Due to its highest cholesterol-complexing ability, MβCD induced the largest concentration-dependent decreases in the

14765381, 0, Downloaded from https://bpspubs.onlinelibrary.wiley.com/doi/10.1111/bph.16063 by Cochrane Hungary, Wiley Online Library on [03/04/2023]. See the Terms and Conditions (https://onlinelibrary.wiley.com/terms-and-conditions) on Wiley Online Library for rules of use; OA articles are governed by the applicable Creative Commons License

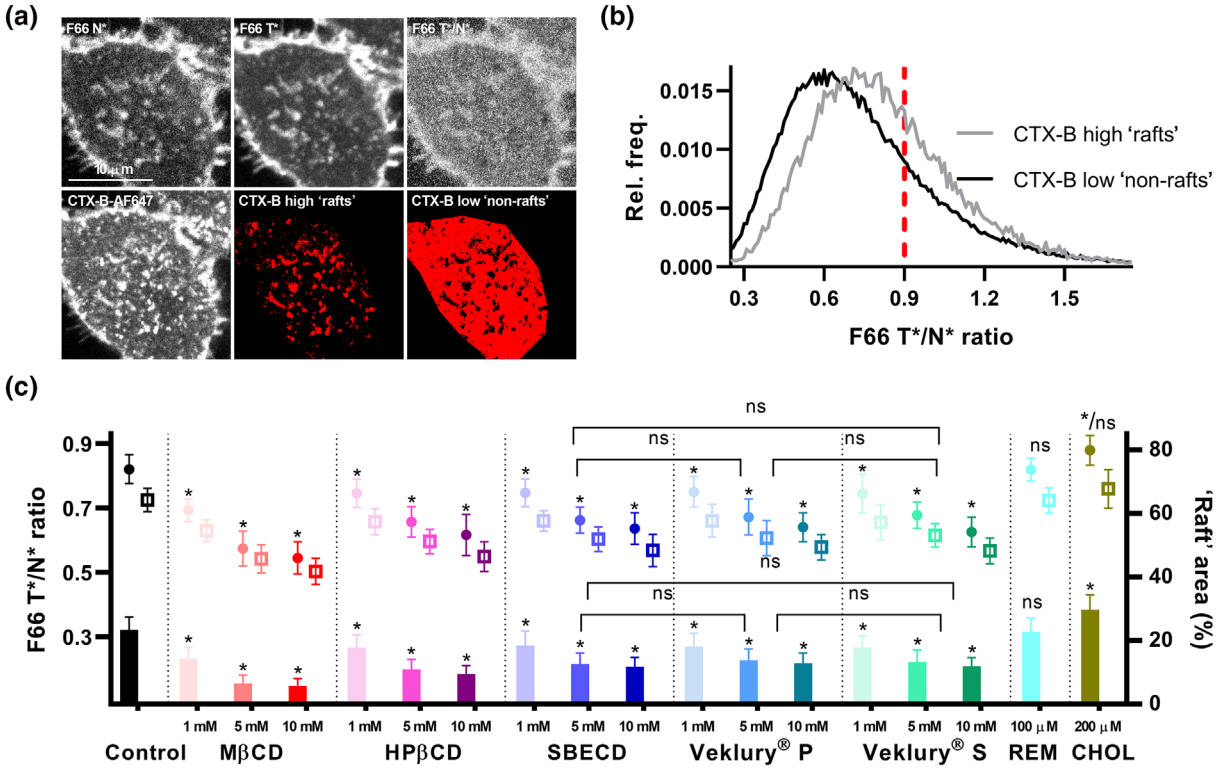


**FIGURE 1** Veklury® (remdesivir) formulations induce alterations in membrane structure and disrupt lipid rafts similarly to cyclodextrins (CDs) in a cholesterol-dependent manner independently of remdesivir. (a) Control HEK/ACE2 + TMPRSS2 cells and those treated with 1-, 5- or 10-mM MβCD, HPβCD, SBECD, Veklury® P (powder) or Veklury® S (solution), 100-µM remdesivir (REM) or 200-µM cholesterol (CHOL) were labelled with cholera toxin subunit B (CTX-B), a lipid raft marker, and *N*-[3-(40-dihexylamino-3-hydroxy-flavonyl-6-oxy)-propyl]*N*,*N*-dimethyl-*N*-(3-sulfopropyl)-ammonium inner salt (F66), an environment-sensitive fluorescent indicator. Representative confocal microscopic images taken from the flat, bottom membrane region adjacent to the coverslip show F66 intensities of the normal (N*) and tautomeric (T*) excited states and the T*/N* emission ratios calculated pixel by pixel. Cell membrane masks selected manually in CTX-B images were segmented using the maxentropy algorithm to 'raft' (CTX-B high) and 'non-raft' (CTX-B low) regions corresponding to high and low intensities of the raft markers, respectively, and average T*/N* intensity ratios were determined separately for the two masks (symbols in [c]). (b) Pixelwise distributions of the T*/N* F66 emission ratio in CTX-B high 'raft' and CTX-B low 'non-raft' regions of control cells are displayed. As an alternative definition for raft regions, a threshold value of the T*/N* ratio was determined (red dashed line) and membrane pixels were considered as 'raft' and 'non-raft' regions when being above and below the threshold, respectively (evaluation shown by the bars in [c]). The threshold value was chosen to result in a segmentation pattern similar to that obtained in (a). (c) The average F66 T*/N* ratios calculated for CTX-B high 'raft' and CTX-B low 'non-raft' pixels (circles and squares, respectively; numerical values to be read on the left vertical axis) as well as the relative fraction of 'raft' pixels (bars, numerical values to be read on the right vertical axis) above the F66 emission ratio threshold (shown by the red line in [b]) were determined in individual cells (n = 20) and the mean ± SD values are plotted. Asterisks indicate significant differences compared to the control samples (*$P < 0.05$; one-way ANOVA followed by Tukey's HSD test). See details of statistical analysis in Table S1.

F66 T*/N* ratios in both raft and non-raft regions. HPβCD also resulted in concentration-dependent reductions that, while being smaller than those after MβCD, were significant even at 1 mM, the smallest applied concentration. Both Veklury® formulations resulted in significantly lower T*/N* values in a concentration-dependent manner both inside and outside rafts, and the changes were of similar magnitude as for HPβCD. When examining SBECD, the vehicle and REM, the active compound alone, changes induced by SBECD were indistinguishable from those after Veklury® P and Veklury® S at identical CD concentrations, whereas REM exerted no significant effects in any membrane regions. In contrast, CHOL significantly increased T*/N* ratios mainly in raft areas. These results supported that CDs significantly modified membrane structure in both lipid raft microdomains and non-raft regions of the cell membrane when applied alone or as Veklury® formulations in a cholesterol-dependent manner.

As an alternative to dividing the membrane to raft and non-raft regions according to their CTX-B binding, we defined lipid rafts utilizing their unique biophysical properties and estimated changes in the fraction of membrane area occupied by these microdomains. We determined a threshold F66 T*/N* ratio based on histograms of CTX-B high and CTX-B low areas of control samples (Figure 1b, red line) and calculated the fraction of membrane pixels above this threshold demonstrating elevated dipole potential. The threshold value was chosen to result in a segmentation pattern similar to that obtained in the first method (Figure 1a). We observed strongly consistent results,

14765381, 0, Downloaded from https://bpspubs.onlinelibrary.wiley.com/doi/10.1111/bph.16063 by Cochrane Hungary, Wiley Online Library on [03/04/2023]. See the Terms and Conditions (https://onlinelibrary.wiley.com/terms-and-conditions) on Wiley Online Library for rules of use; OA articles are governed by the applicable Creative Commons License

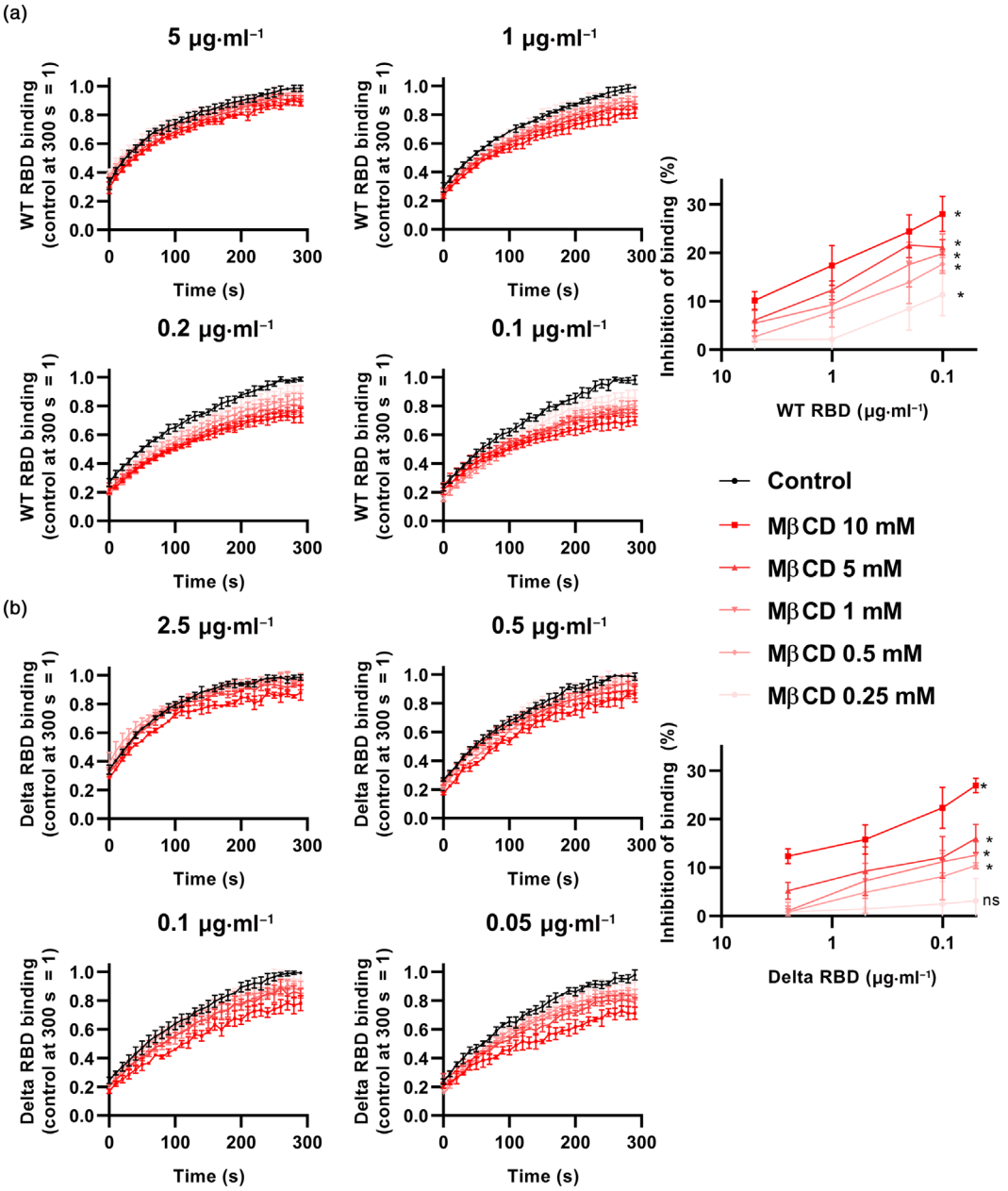


**FIGURE 2** Methyl-β cyclodextrin (MβCD)-induced reductions in ACE2 binding of Wuhan-Hu-1 strain of SARS-CoV-2 (WT) and Delta SARS-CoV-2 spike receptor-binding domains (RBDs) negatively correlate with the applied RBD concentrations. HEK/ACE2 + TMPRSS2 cells were treated with different concentrations of MβCD ranging between 0.25 and 10 mM. Fluorescence intensities of cells were measured using flow cytometry for 5 min continuously starting immediately after the addition of GFP-conjugated WT (a) or Delta (b) SARS-CoV-2 spike RBDs applied at various concentrations between 0.1 and 5 μg·ml$^{-1}$, or 0.05 and 2.5 μg·ml$^{-1}$, respectively. Moving averages of time-correlated fluorescence intensities of at least 50,000 cells of normal morphology were determined with a window size of 10 s and subsequently normalized to the average of intensities obtained in the last time window of untreated control samples. Mean ± SD values were calculated from data of six independent samples per treatment condition and plotted as a function of time (starting ~20 s after RBD addition). The extents of inhibition of WT (a) and Delta (b) RBD binding at the end of the measurement time in response to various MβCD concentrations were calculated and plotted as mean ± SD as a function of the applied RBD concentration in the right panels. Asterisks indicate significant differences of samples treated with the lowest versus highest RBD concentrations at each applied CD concentration (*$P$ < 0.05; two-way ANOVA followed by Tukey's HSD test). See details of statistical analysis in Table S2.

as MβCD, HPβCD, SBECD, Veklury® P and Veklury® S significantly and concentration-dependently reduced the relative area occupied by lipid rafts, whereas REM had no effects and CHOL increased it (Figure 1c columns and Table S1). These findings support that Veklury® formulations, independent of their remdesivir content, induce significant alterations in membrane structure and lipid raft integrity, similarly to cholesterol-depleting CDs and contrary to cholesterol loading.

14765381, 0, Downloaded from https://bpspubs.onlinelibrary.wiley.com/doi/10.1111/bph.16063 by Cochrane Hungary, Wiley Online Library on [03/04/2023]. See the Terms and Conditions (https://onlinelibrary.wiley.com/terms-and-conditions) on Wiley Online Library for rules of use; OA articles are governed by the applicable Creative Commons License

### 3.2 | Veklury® (remdesivir) formulations decrease ACE2 binding of Wuhan-Hu-1 strain (WT) and Delta SARS-CoV-2 spike receptor-binding domains (RBDs) correlating with their SBECD content

To investigate whether CD-induced alterations in membrane structure influence the first step in the interaction of SARS-CoV-2 with cells, we studied the cellular binding of WT and Delta SARS-CoV-2 spike RBDs conjugated with GFP. First, using confocal microscopy, we demonstrated that these RBDs bind to the membrane of HEK/ACE2 + TMPRSS2 cells after 5 min of incubation. On the contrary, RBDs fail to interact with HEK cells that do not express ACE2 (Figure S1A–C). Next, we followed the time dependence of RBD binding using a time-correlated flow cytometry method (Batta et al., 2021) by measuring the fluorescence intensity of individual cells with a normal morphology immediately after RBD addition for up to 5 min. Although this method did not provide information about the first ~20 s of incubation due to technical limitations, it precisely and reproducibly characterized the following 5 min of RBD binding. These experiments demonstrated that a considerable amount of RBD is bound to the cells even after short incubation, which depended on incubation time, the RBD concentration and the type of RBD because, consistent with previously published results (Wang et al., 2022; Yang et al., 2021), binding of the Delta variant was superior to that of the WT at a given RBD concentration (Figure S1D). MβCD, the CD with the highest efficiency to induce membrane structure alterations, significantly inhibited cellular binding of both WT and Delta RBDs in a concentration-dependent manner and the extents of MβCD-induced reductions showed negative correlation with the amount of applied RBD in both examined variants (Figure 2 and Table S2). In particular, 10-mM MβCD hindered WT RBD binding by 10%–12% at the highest applied RBD concentration and the inhibitory effect increased to 27%–28% at the lowest examined RBD concentration. Binding of the WT RBD was consistently more sensitive to MβCD-induced inhibition than that of the Delta variant. These findings have two important consequences: (i) because the experimentally applied RBD/spike concentrations are higher than those reached *in vivo*, effects induced by MβCD are expected to be much larger at medically relevant RBD/spike concentrations (see calculations in Section 4 for further details); and (ii) it is advisable to examine RBD binding at as low RBD concentrations as permitted by methodological limitations. Therefore, we carried out subsequent experiments at the lowest possible RBD/trimer concentrations with still adequate signal-to-noise ratios. These results suggested that the cholesterol-complexing MβCD efficiently decreases RBD binding of both variants to the cell surface.

To compare the ability of Veklury® formulations and medically more relevant CDs, such as SBECD and HPβCD, to that of MβCD to inhibit cellular binding of WT (0.2 μg·ml$^{-1}$) and Delta (0.1 μg·ml$^{-1}$) RBDs, we quantified cell-bound fluorescence signals in HEK/ACE2 + TMPRSS2 cells after 4-min incubation in the presence of RBDs using flow cytometry applying a dilution series of CD concentrations between 0.078 and 20 mM. MβCD concentration-dependently lowered binding of both WT and Delta RBDs with the effects slightly larger in the former with maximal reductions of 35% and 23%, respectively (Figure 3a left panels and Table S3). HPβCD treatment resulted in similar changes, albeit of smaller magnitude, and consistent with the previous experiments, SBECD, Veklury® P and Veklury® S significantly decreased binding of both WT and Delta RBDs with a maximal inhibition observed at 20 mM ranging between 17%–21% and 13%–16% for WT and Delta RBDs, respectively. CD-induced effects showed statistical significance above 0.625–1.25 mM, whereas no significant difference was obtained between SBECD, Veklury® P and Veklury® S at identical CD concentrations. Consistent with our hypothesis that the SBECD content of the Veklury® formulations is the active component in this aspect, REM alone did not result in significant effects on RBD binding even at 1200-μM concentration. An alternative presentation of data, where the effects of Veklury® P and Veklury® S were compared at identical remdesivir concentrations (Figure 3a right panels), showed that Veklury® S was significantly more effective compared to Veklury® P in inhibiting the binding of both RBD variants. This phenomenon can be the consequence of the higher relative SBECD content of Veklury® S. If this assumption was true, then supplementing Veklury® P with SBECD should increase its potency in modulating RBD binding. To this end, we performed RBD binding assays using Veklury® P supplemented with SBECD in a 1:1 (w/w) ratio, which brings the SBECD concentration of the mixture to that of Veklury® S and found that the effects of the mixture were quantitatively identical to those caused by Veklury® S using either RBD variants. On the other hand, CHOL elevated binding of both WT and Delta RBDs in a concentration-dependent manner with maximal effects of 7%–8% at the highest applied dose of 800 μM and changes being significant above 100 and 200 μM, respectively, corroborating the cholesterol dependence of RBD binding to ACE2.

Because ACE2- and TMPRSS2-overexpressing HEK cell lines, most widely used in *in vitro* SARS-CoV-2 studies, are characterized by supraphysiological ACE2 and TMPRSS2 levels, the measurements were repeated in Calu-3 cells with lower level of endogenous ACE2 expression, thereby presenting a medically more relevant model system. Accordingly, we observed lower degree of membrane binding of SARS-CoV-2 RBDs (Figure S2). In general, as shown in Figure 3b and Table S3, the changes in RBD binding induced by the treatments strongly correlated with those observed in HEK/ACE2 + TMPRSS2 cells and were even of higher magnitude, although much higher RBD concentrations were required for the measurements in Calu-3 (1.0 and 0.5 μg·ml$^{-1}$ for WT and Delta variants, respectively). All of the examined CDs including MβCD, HPβCD and SBECD, both Veklury® P and Veklury® S, and the Veklury® P:SBECD mixture effectively and dose-dependently blocked WT RBD binding with maximal reductions of 41%–50% and inhibition being statistically significant above 0.625–1.25 mM (Figure 3b left panels). Again, REM failed to change WT RBD binding significantly, whereas CHOL elevated it (maximal effect of 30% at 800 μM and significant changes above 200 μM) (Figure 3b right panels). We observed no statistically significant differences between alterations in response to SBECD, Veklury®

14765381, 0, Downloaded from https://bpspubs.onlinelibrary.wiley.com/doi/10.1111/bph.16063 by Cochrane Hungary, Wiley Online Library on [03/04/2023]. See the Terms and Conditions (https://onlinelibrary.wiley.com/terms-and-conditions) on Wiley Online Library for rules of use; OA articles are governed by the applicable Creative Commons License

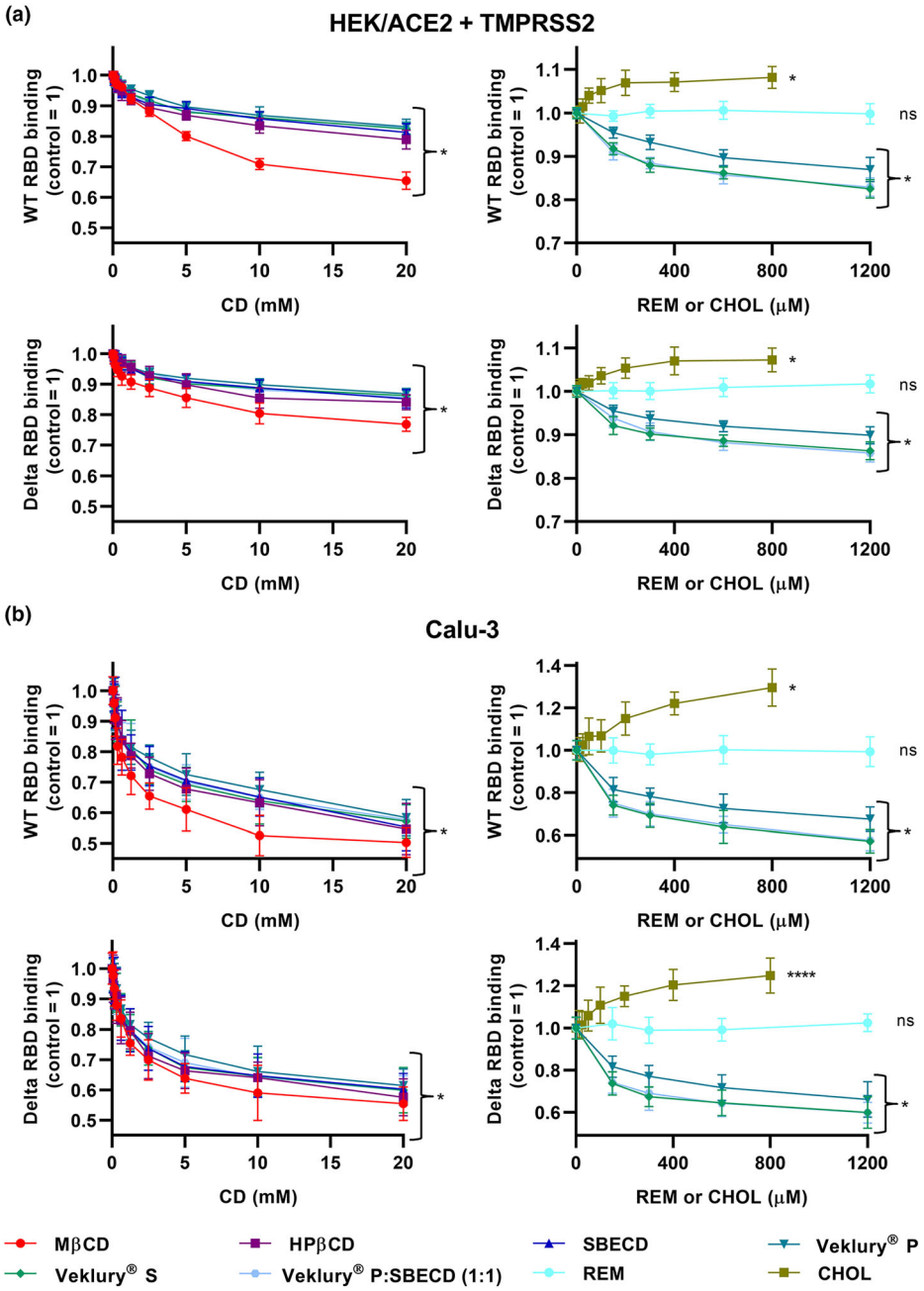


**FIGURE 3** Veklury® (remdesivir) formulations and cyclodextrin (CDs) reduce the cellular binding of Wuhan-Hu-1 strain of SARS-CoV-2 (WT) and Delta SARS-CoV-2 spike receptor-binding domain (RBDs) in a cholesterol-dependent manner. HEK/ACE2 + TMPRSS2 (a) or Calu-3 (b) cells were treated with a dilution series of MβCD, HPβCD, SBECD, Veklury® P (powder), Veklury® S (solution) or a 1:1 (w/w) mixture of Veklury® P and SBECD at CD concentrations ranging between 0.078 and 20 mM, remdesivir (REM) between 75 and 1200 μM or cholesterol (CHOL) between 12.5 and 800 μM. HEK/ACE2 + TMPRSS2 cells were incubated in the presence of 0.2-μg·ml$^{-1}$ WT or 0.1-μg·ml$^{-1}$ Delta SARS-CoV-2 spike RBD–GFP, whereas Calu-3 cells were labelled with 1-μg·ml$^{-1}$ WT or 0.5-μg·ml$^{-1}$ Delta RBD–GFP for 4 min. The emitted fluorescence intensities of individual cells were subsequently measured using flow cytometry and the mean intensity was calculated from data of at least 10,000 cells of normal morphology per sample. The average values of six independent measurements (±SD) were calculated, normalized to the mean value determined in untreated control samples and plotted as a function of the applied concentrations of CD (in the left panels) and CHOL or REM (in the right panels). Asterisks indicate significant differences of samples treated with the highest applied concentrations compared to the control samples (*$P < 0.05$; two-way ANOVA followed by Tukey's HSD test). See details of statistical analysis in Table S3.

P, Veklury® S and Veklury® P:SBECD at identical CD concentrations (Figure 3b left panels), whereas at a given applied remdesivir concentration, Veklury® S and Veklury® P:SBECD were more effective than Veklury® P (Figure 3b right panels). Strongly consistent changes were found when examining Delta RBD, as MβCD, HPβCD, SBECD, Veklury® P, Veklury® S and Veklury® P:SBECD decreased RBD binding

14765381, 0, Downloaded from https://bpspubs.onlinelibrary.wiley.com/doi/10.1111/bph.16063 by Cochrane Hungary, Wiley Online Library on [03/04/2023]. See the Terms and Conditions (https://onlinelibrary.wiley.com/terms-and-conditions) on Wiley Online Library for rules of use; OA articles are governed by the applicable Creative Commons License

(maximal effects of 38%–45%, significant changes above 0.625–1.25 mM), whereas REM induced no changes and CHOL increased it (maximal effect of 25%, significant changes above 200 μM). Again, no differences were observed between SBECD, Veklury® P, Veklury® S and Veklury® P:SBECD at a given CD concentration and the effects of Veklury® S and Veklury® P:SBECD were superior to those of Veklury® P at identical remdesivir concentrations. In general, the effects were larger for WT RBD compared to Delta. These results strongly support that Veklury® formulations can reduce ACE2 binding of both WT and Delta RBDs via their cholesterol-extracting effects, which is independent of remdesivir. Furthermore, Veklury® S was more effective than Veklury® P due to its higher SBECD content.

### 3.3 | Both Veklury® (remdesivir) formulations and CDs reduce cell surface expression of ACE2 and its colocalization with lipid rafts and TMPRSS2

To investigate possible mechanisms contributing to inhibition of SARS-CoV-2 spike RBD binding to the cell membrane, first, we examined possible changes in the cell surface expression of ACE2 because previous studies suggested that reduced membrane cholesterol levels in response to MβCD or statin treatment result in lower ACE2 levels in the cell membrane (Teixeira et al., 2022; Wang et al., 2021). Consistent with these studies, we observed concentration-dependent reductions of ACE2 levels in the cell membrane after treating HEK/ACE2 + TMPRSS2 cells with MβCD, HPβCD, SBECD, Veklury® P and Veklury® S. The dose-dependent changes were already significant at the lowest examined concentration of 1-mM CD and increased up to a 23%–42% reduction in ACE2 expression at the highest applied dose of 10-mM CD (Figure 4a and Table S4). On the other hand, REM did not change ACE2 level significantly, whereas 200-μM CHOL increased it by 16%. These data support that the amount of membrane cholesterol positively correlates with the extent of ACE2 localization on the cell surface and, therefore, the efficiency of binding of the SARS-CoV-2 spike RBD to target cells.

Lipid raft microdomains of the cell membrane are characterized by a unique composition with high levels of cholesterol and the preferential accumulation of certain transmembrane proteins. Therefore, CDs having the ability to extract cholesterol from the cell membrane can induce lipid raft disruption and consequent changes in the distribution of various cell surface receptors (Kovacs et al., 2022; Palacios-Rápalo et al., 2021; Sezgin et al., 2017; Wang et al., 2021; Zakany et al., 2020; Zidovetzki & Levitan, 2007). To test the hypothesis that Veklury® formulations and cholesterol-complexing CDs can affect lateral distribution of ACE2 and TMPRSS2, we evaluated their ability to modify the lipid raft partitioning of ACE2 and TMPRSS2 in the plasma membrane of HEK/ACE2 + TMPRSS2 cells. Using confocal microscopy and quantitative image analysis, we determined the Pearson correlation coefficients between the intensities of fluorophores visualizing lipid rafts, ACE2 and TMPRSS2, which quantify the extents of colocalization of the labelled objects. In control cells, the strongly positive correlation coefficients between lipid rafts and ACE2 or TMPRSS2 suggested that these two proteins are preferentially localized in lipid rafts (Figure 4b,c and Table S4). Similarly, a positive correlation was found between ACE2 and TMPRSS2, suggesting that these proteins tend to localize in the vicinity of each other, and this proximity can contribute to the generation of platforms with multiple viral entry points organized by lipid rafts (Figure 4d and Table S4). The statistical significance of the observed colocalizations is supported by the fact that the calculated coefficients were far outside the 95% confidence intervals determined when assuming the absence of correlation (Figure 4b–d, grey shaded areas). When examining colocalization parameters after CD treatments, we observed CD-induced changes that strongly correlated with alterations induced in lipid raft integrity (Figure 1c) because all CDs as well as both Veklury® formulations significantly lowered Pearson coefficients between lipid raft, ACE2 and TMPRSS2 signals in a concentration-dependent manner. MβCD induced changes of the largest magnitude, whereas HPβCD, SBECD, Veklury® P and Veklury® S exerted alterations of similar extent, as no significant differences were observed between these samples at any examined concentration. On the other hand, REM did not change any of the coefficients significantly, whereas CHOL treatment resulted in significantly higher colocalizations. These results strongly support our hypothesis that lipid raft disruption induced by Veklury® formulations and cholesterol-complexing CDs is accompanied by a modified lateral distribution of ACE2 and TMPRSS2 characterized by decreased raft partitioning of these proteins. Furthermore, the lower ACE2–TMPRSS2 colocalization suggests that their decreased vicinity in the cell membrane could lead to a reduced efficiency of the TMPRSS2-mediated cellular entry pathway in response to these treatments.

### 3.4 | Veklury® (remdesivir) formulations and cholesterol-complexing CDs decrease cellular uptake of WT and Delta SARS-CoV-2 spike trimers

In addition to the cellular entry pathway mediated by cell surface proteases, SARS-CoV-2 can enter cells via endocytosis and subsequent trimer cleavage by cathepsins in endosomal compartments (Bayati et al., 2021; Jackson et al., 2022; Li et al., 2021; Ou et al., 2020). Because endocytic mechanisms including raft- and clathrin-mediated endocytosis generally depend on membrane cholesterol levels (Ripa et al., 2021), Veklury® formulations and cholesterol-complexing CDs can alter the efficiency of these processes as well. To examine this eventuality, we incubated cells for 4 h in the presence of WT or Delta trimers (0.5 and 0.25 $\mu g \cdot ml^{-1}$, respectively) conjugated with Alexa Fluor 488 and examined them with a confocal microscope. First, we demonstrated that trimers are selectively bound to HEK/ACE2 + TMPRSS2 cells and internalized by the end of the incubation whereas binding and internalization were absent when WT HEK cells lacking the ACE2 and TMPRSS2 were used (Figure S3). For quantitative analysis of trimer uptake, we recorded Z-stack images containing 15–20 slices from cells treated with Veklury® formulations, CDs, REM

14765381, 0, Downloaded from https://bpspubs.onlinelibrary.wiley.com/doi/10.1111/bph.16063 by Cochrane Hungary, Wiley Online Library on [03/04/2023]. See the Terms and Conditions (https://onlinelibrary.wiley.com/terms-and-conditions) on Wiley Online Library for rules of use; OA articles are governed by the applicable Creative Commons License

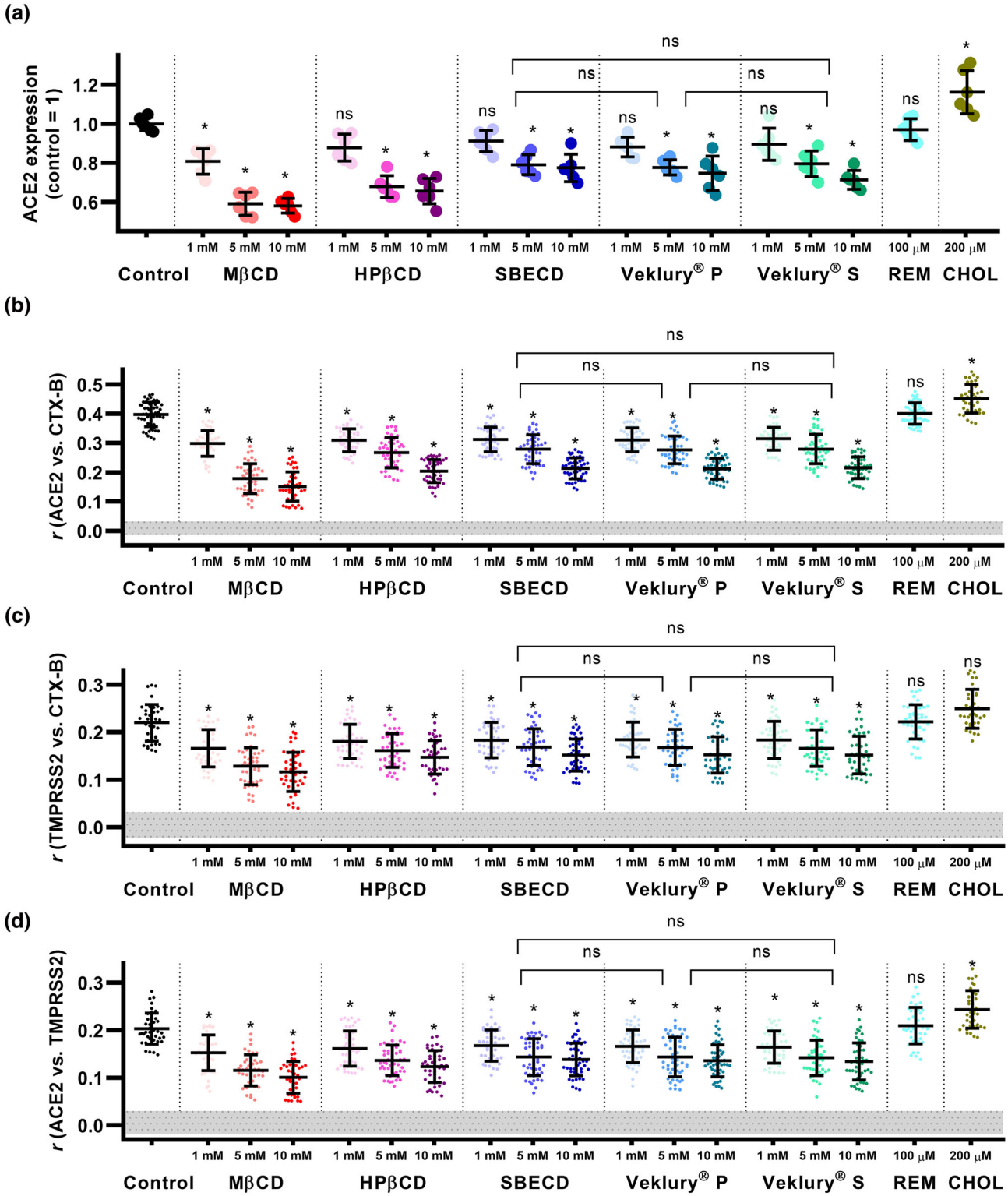


**FIGURE 4** Legend on next page.

14765381, 0, Downloaded from https://bpspubs.onlinelibrary.wiley.com/doi/10.1111/bph.16063 by Cochrane Hungary, Wiley Online Library on [03/04/2023]. See the Terms and Conditions (https://onlinelibrary.wiley.com/terms-and-conditions) on Wiley Online Library for rules of use; OA articles are governed by the applicable Creative Commons License

or CHOL and incubated in the presence of WT or Delta trimers. The cell membrane was visualized using F66 for determination of the Alexa Fluor 488 signal originating from internalized trimers (Figure 5a). After identifying cell membrane and intracellular pixels using a 3D watershed algorithm based on F66 images (Figure 5b), we determined the average Alexa Fluor 488 intensity characterizing the amount of internalized trimers using data of intracellular pixels for each cell. In these experiments, MβCD concentration-dependently decreased the uptake of both WT and Delta trimers, reaching 52% and 58% at the highest examined dose of 5 mM, respectively, when compared to controls (Figure 5c and Table S5). Similarly, HPβCD, SBECD, Veklury® P and Veklury® S also concentration-dependently inhibited internalization of both variants, with maximal reductions to 66%–68% and 69%–74% at 5 mM, respectively, for WT and Delta trimers. All of the observed CD-induced changes were found statistically significant at both 1 and 5 mM for all compounds, whereas no significant differences were observed between SBECD, Veklury® P and Veklury® S at any given CD concentration. On the contrary, REM did not modify the uptake of any variants, whereas CHOL significantly stimulated it by 21%–23%.

We repeated the measurements in Calu-3 cells (with 2.5-μg·ml$^{-1}$ WT and 1.25-μg·ml$^{-1}$ Delta trimers) and observed results in a good agreement with those in HEK/ACE2 + TMPRSS2 (Figure 5d and Table S5). Notably, all CDs and both Veklury® formulations effectively and dose-dependently inhibited internalization of both trimers with significant effects at both 1 and 5 mM. In general, reductions of internalization were higher in Calu-3 cells (at 5-mM CD, trimer uptake was reduced to 46%–58% for WT and 53%–67% for Delta) than in HEK/ACE2 + TMPRSS2 (for WT, significant differences were found between the two cell types after all examined CDs, whereas for Delta, in the cases of HPβCD and Veklury® P; $P < 0.05$). Again, no significant differences were found between SBECD, Veklury® P and Veklury® S. REM failed to modify WT or Delta trimer uptake, whereas CHOL resulted in significant increases to 117% and 111%, respectively. These results convincingly suggest that Veklury® formulations and cholesterol-complexing CDs inhibit internalization of both WT and Delta trimers and, therefore, can modify endocytosis-dependent cellular entry pathways of SARS-CoV-2.

### 3.5 | Veklury® (remdesivir) formulations and SBECD retain their ability to inhibit ACE2 binding and cellular internalization of the Omicron variant

To test if Veklury® formulations can also interfere with membrane binding and cellular internalization of newly emerging SARS-CoV-2 variants in an SBECD content-dependent manner, we performed the same experiments shown in Figures 3 and 5 using fluorophore-conjugated Omicron Ba1 RBDs and trimers, and applied Veklury® P, Veklury® S and SBECD at CD concentrations of 1, 5 and 10 mM. When examining cell surface binding of GFP-conjugated Omicron RBD (0.2 μg·ml$^{-1}$) in HEK/ACE2 + TMPRSS2 cells, we observed that Veklury® P and Veklury® S, and also SBECD reduced Omicron RBD binding in a CD concentration-dependent manner (Figure 6a left panel and Table S6). The extents of inhibition were similar to those observed previously with the other RBDs, with an inhibition of ~15% at the maximal applied CD concentration of 10 mM and significant changes even at the lowest tested concentration of 1 mM. Similar to the observations with the WT and Delta RBD variants, the magnitude of inhibition of Omicron RBD binding (1 μg·ml$^{-1}$) to Calu-3 cells induced by the treatments was higher than in HEK/ACE2 + TMPRSS2 cells with an inhibition of ~35% after 10 mM (Figure 6a right panel and Table S6). In both cell types, Veklury® P, Veklury® S and SBECD exerted quantitatively indistinguishable effects indicating that the action is related to the CD content of the treatments.

Next, we examined if Veklury® P, Veklury® S and SBECD applied at 1- and 5-mM CD concentrations can interfere with the cellular entry of Alexa Fluor 488-conjugated Omicron trimer. In these experiments, we used the confocal microscope-based quantitative 3D approach as described above (Figure 5 and the corresponding results). In harmony with the results obtained for WT and Delta trimers in HEK/ACE2 + TMPRSS2 cells, Veklury® P, Veklury® S and SBECD concentration-dependently reduced the uptake of the Omicron trimer (0.5 μg·ml$^{-1}$) as well, with an ~40% decrease at 5-mM CD (Figure 6b left panel and Table S6). A similar, dose-dependent inhibition of Omicron trimer (2.5 μg·ml$^{-1}$) internalization was observed in Calu-3 cells (Figure 6b right panel and Table S6). In both cell types, reductions were statistically significant even at 1-mM CD. Changes induced by

**FIGURE 4** Veklury® (remdesivir) formulations and cyclodextrins (CDs) decrease cell surface ACE2 expression and colocalization between lipid rafts, ACE2 and TMPRSS2. (a) HEK/ACE2 + TMPRSS2 cells were treated with 1-, 5- or 10-mM MβCD, HPβCD, SBECD, Veklury® P (powder) or Veklury® S (solution), 100-μM remdesivir (REM) or 200-μM cholesterol (CHOL), and the levels of cell surface ACE2 were examined using Alexa Fluor 488-conjugated anti-ACE2 antibodies and flow cytometry. The mean intensity was calculated from data of at least 10,000 cells of normal morphology per sample and subsequently normalized to the mean value determined in untreated control samples. The average values of six independent measurements (±SD) were calculated and plotted in the figure in addition to mean values of individual samples. Control cells and those treated as above were labelled with cholera toxin subunit B (CTX-B) and anti-ACE2 antibody (b), CTX-B and anti-TMPRSS2 antibody (c), or anti-ACE2 and anti-TMPRSS2 antibodies (d), and the Pearson correlation coefficient values between fluorescence intensities of the two applied fluorophores were determined from pixelwise data of individual cells and plotted as mean ± SD in addition to values of individual cells. The number of cells obtained from five independent experiments and involved in the analysis was from left to right: 52, 44, 47, 42, 44, 45, 46, 46, 46, 48, 47, 44, 46, 43, 45, 48, 53 and 41 for CTX-B versus anti-ACE2; 40, 40, 46, 45, 44, 45, 40, 40, 44, 47, 41, 40, 41, 44, 42, 42, 46 and 40 for CTX-B versus anti-TMPRSS2; and 40, 44, 41, 41, 45, 51, 44, 44, 47, 47, 47, 50, 51, 43, 46, 47, 40 and 40 for anti-ACE2 versus anti-TMPRSS2. The 95% confidence interval of the coefficient assuming no correlation was determined for each image and its mean values were displayed as grey dotted areas. Asterisks indicate significant differences compared to the control samples (*$P < 0.05$; one-way ANOVA followed by Tukey's HSD test). See details of statistical analysis in Table S4.

14765381, 0, Downloaded from https://bpspubs.onlinelibrary.wiley.com/doi/10.1111/bph.16063 by Cochrane Hungary, Wiley Online Library on [03/04/2023]. See the Terms and Conditions (https://onlinelibrary.wiley.com/terms-and-conditions) on Wiley Online Library for rules of use; OA articles are governed by the applicable Creative Commons License

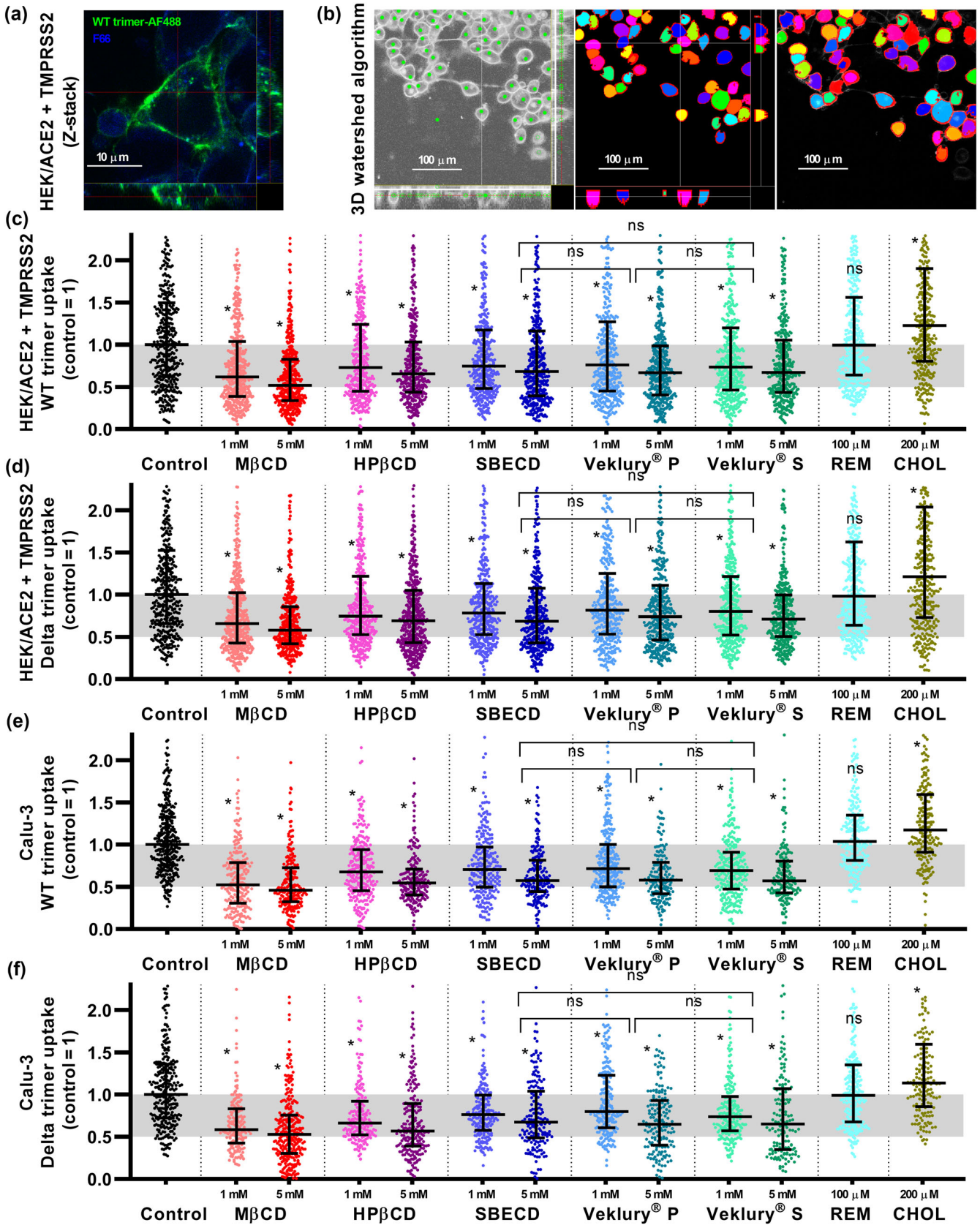


**FIGURE 5** Legend on next page.

14765381, 0, Downloaded from https://bpspubs.onlinelibrary.wiley.com/doi/10.1111/bph.16063 by Cochrane Hungary, Wiley Online Library on [03/04/2023]. See the Terms and Conditions (https://onlinelibrary.wiley.com/terms-and-conditions) on Wiley Online Library for rules of use; OA articles are governed by the applicable Creative Commons License

Veklury® P, Veklury® S and SBECD were statistically equivalent in both cell types and CD concentrations. These results convincingly suggest that Veklury® formulations, as a consequence of their SBECD content, retain their ability to inhibit cholesterol-dependent membrane-coupled events of infection in recent and potential future SARS-CoV-2 variants.

## 4 | DISCUSSION

As a major finding of our experiments, we demonstrated previously unexplored effects of Veklury® formulations to inhibit initial cholesterol-dependent membrane-coupled events of cellular SARS-CoV-2 infection due to solely their sulfobutylether-β-cyclodextrin (SBECD) content, which can contribute to the action of Veklury® independent of remdesivir and potentially enhancing its antiviral effects. Initial stages of virus–host cell interactions include the following: (i) binding of the spike glycoprotein to ACE2 (Hoffmann et al., 2020; Jackson et al., 2022; Zhou et al., 2020), (ii) its cleavage by TMPRSS2 on the cell surface (Hoffmann et al., 2020; Jackson et al., 2022) or (iii), endocytosis of virions followed by spike cleavage by **cathepsins** (Hoffmann et al., 2020; Jackson et al., 2022; Ou et al., 2020). The SBECD component present at high levels in both Veklury® formulations targets all of these early events, which was revealed by showing reduced binding of RBD (Figures 2 and 3) and diminished internalization of spike trimers (Figure 5) after CD or Veklury® treatments. Inhibition of RBD binding may be caused by CD-induced reduced cell surface expression and raft localization of ACE2 (Figure 4a,b), whereas reduced trimer internalization is likely the consequence of the cholesterol dependence of endocytic uptake. Furthermore, the close vicinity of TMPRSS2 and the viral spike, required for cleavage and brought about by the raft-dependent colocalization between the TMPRSS2 and ACE2, was also abolished by cholesterol extraction (Figure 4c,d). Not only did Veklury® formulations and SBECD effectively inhibit membrane binding and cellular entry of WT and Delta variants, these treatments were similarly effective for the Omicron variant also characterized by a cholesterol-dependent cellular uptake (Figure 6). Although the applied methods do not allow insight into later steps of infection, that is, protease cleavage of the spike, membrane fusion, viral RNA replication and virion release, the specific and quantitative investigation of the crucial initial stages of the infection cycle provides much needed information about this less intensively studied aspect. The fact that Veklury® formulations, just as cholesterol-complexing CDs, inhibited all the crucial initial steps of virus–host cell interactions calls for a consideration of additional CD-induced actions in the *in vivo* antiviral effects of Veklury® and the discrimination of the two formulations in light of their different SBECD content.

Several lines of evidence suggest that reduced membrane cholesterol levels in general and the SBECD component of Veklury® formulations in particular, inhibit binding and uptake of SARS-CoV-2:-

a. SBECD, Veklury® P and Veklury® S actions are indistinguishable at identical CD concentrations and REM alone did not induce any alterations (Figures 3–5). Furthermore, quantitative flow cytometric comparison of Veklury® P and Veklury® S effects at identical remdesivir concentrations demonstrated that Veklury® S is superior to Veklury® P. The effects of Veklury® P were boosted by SBECD supplementation because the 1:1 (w/w) Veklury® P:SBECD mixture exerted an RBD binding inhibition quantitatively identical to that in response to Veklury® S (Figure 3). These data collectively argue that Veklury® S is superior to Veklury® P due to its doubled SBECD content. The limited cell numbers (technical limitation) and relatively large deviations in fluorescence intensities of individual cells prevented us from performing such a comparison in confocal microscopy. However, these findings altogether strongly propose the favourable effects of Veklury® S over Veklury® P on the examined parameters.

**FIGURE 5** Veklury® (remdesivir) formulations and cyclodextrins (CDs) inhibit the internalization of WT and Delta SARS-CoV-2 spike trimers in a cholesterol-dependent manner. HEK/ACE2 + TMPRSS2 or Calu-3 cells treated with 1- or 5-mM MβCD, HPβCD, SBECD, Veklury® P (powder) or Veklury® S (solution), 100-μM remdesivir (REM) or 200-μM cholesterol (CHOL) for 1 h were subsequently incubated for 4 h in the presence of WT or Delta SARS-CoV-2 spike trimers conjugated with Alexa Fluor 488 and labelled with *N*-[3-(40-dihexylamino-3-hydroxy-flavonyl-6-oxy)-propyl]*N*,*N*-dimethyl-*N*-(3-sulfopropyl)-ammonium inner salt (F66). (a) A representative orthogonal view of a confocal Z-stack of untreated control HEK/ACE2 + TMPRSS2 cells demonstrates notable internalization of trimers. (b) During image analysis, pixels corresponding to plasma membrane and intracellular pixels were identified in F66 Z-stack images. Markers were placed inside cells (green circles in the grayscale orthogonal view), and a MATLAB implementation of the 3D watershed algorithm identified the intracellular space of cells and their membrane (coloured regions and red lines in the orthogonal view in the middle, respectively, and their overlay image displayed on the right). The average fluorescence intensity values emitted by Alexa Fluor 488-labelled trimers were calculated using data of intracellular pixels for individual HEK/ACE2 + TMPRSS2 (c, d) and Calu-3 cells (e, f) for WT and Delta spike trimers, respectively, which were subsequently normalized to the median value determined in untreated control samples. The number of cells obtained from five independent experiments and involved in the analysis was from left to right: 411, 471, 411, 362, 377, 411, 413, 379, 417, 424, 374, 398 and 365 for WT trimer uptake in HEK/ACE2 + TMPRSS2; 409, 469, 411, 389, 452, 404, 407, 367, 398, 398, 383, 403 and 368 for Delta trimer uptake in HEK/ACE2 + TMPRSS2; 266, 228, 217, 256, 198, 238, 183, 218, 161, 264, 154, 249 and 202 for WT trimer uptake in Calu-3; and 242, 168, 235, 184, 202, 216, 171, 208, 166, 215, 154, 264 and 166 for Delta trimer uptake in Calu-3. Data points indicated in the figure were obtained from individual cells and plotted along with median values with quartiles. Grey shaded areas show ranges between 0.5 and 1. Asterisks indicate significant differences compared to the control samples (*$P < 0.05$; one-way ANOVA followed by Tukey's HSD test). See details of statistical analysis in Table S5.

14765381, 0, Downloaded from https://bpspubs.onlinelibrary.wiley.com/doi/10.1111/bph.16063 by Cochrane Hungary, Wiley Online Library on [03/04/2023]. See the Terms and Conditions (https://onlinelibrary.wiley.com/terms-and-conditions) on Wiley Online Library for rules of use; OA articles are governed by the applicable Creative Commons License

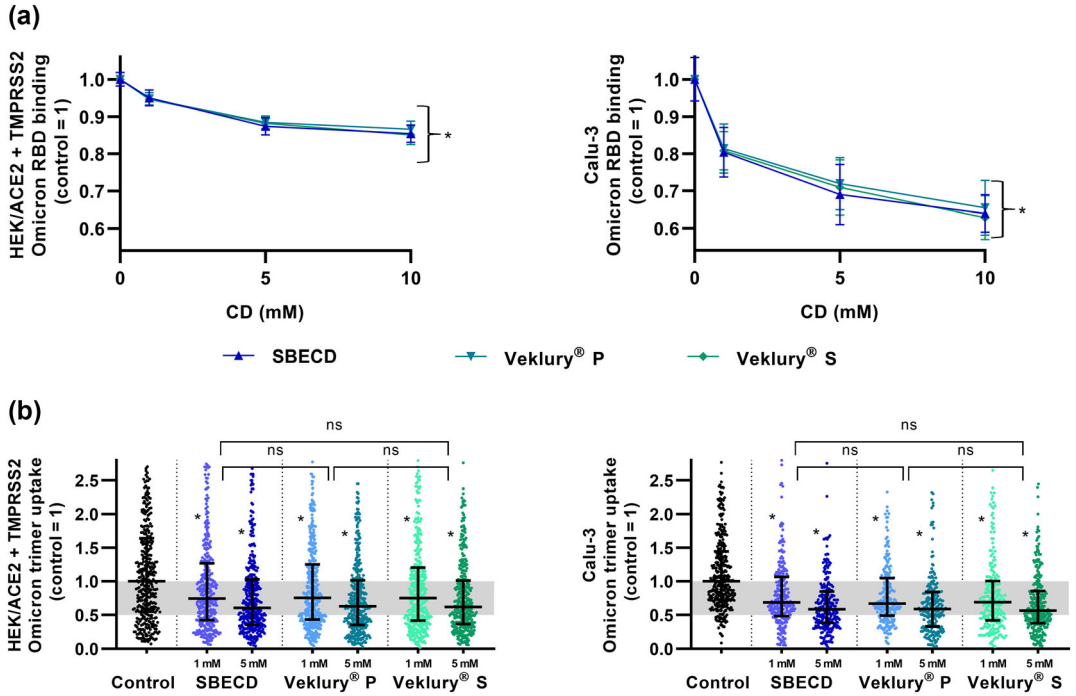


**FIGURE 6** Veklury® (remdesivir) formulations effectively decrease ACE2 binding of Omicron SARS-CoV-2 spike receptor-binding domain (RBD) and the cellular uptake of Omicron SARS-CoV-2 spike trimer due to their SBECD content. (a) HEK/ACE2 + TMPRSS2 (left panel) or Calu-3 cells (right panel) were treated with SBECD, Veklury® P (powder) or Veklury® S (solution) at CD concentrations of 1, 5 and 10 mM. Then, HEK/ACE2 + TMPRSS2 cells were incubated in the presence of 0.2-μg·ml$^{-1}$ Omicron SARS-CoV-2 spike RBD–GFP, whereas Calu-3 cells were labelled with 1-μg·ml$^{-1}$ Omicron RBD–GFP for 4 min. The emitted fluorescence intensities of individual cells were subsequently measured using flow cytometry, and the mean intensity was calculated from data of at least 10,000 cells of normal morphology per sample. The average values of six independent measurements (±SD) were calculated, normalized to the mean value determined in untreated control samples and plotted as a function of the applied concentrations of CD. Asterisks indicate significant differences of samples treated with the highest applied concentrations compared to the control samples (*$P$ < 0.05; two-way ANOVA followed by Tukey's HSD test). See details of statistical analysis in Table S6. (b) HEK/ACE2 + TMPRSS2 (left panel) or Calu-3 cells (right panel) treated with SBECD, Veklury® P or Veklury® S at CD concentrations of 1 and 5 mM for 1 h were subsequently incubated for 4 h in the presence of Omicron SARS-CoV-2 spike trimers conjugated with Alexa Fluor 488. The average fluorescence intensity values emitted by Alexa Fluor 488-labelled trimers were calculated using data of intracellular pixels identified using the membrane marker *N*-[3-(40-dihexylamino-3-hydroxy-flavonyl-6-oxy)-propyl]*N*,*N*-dimethyl-*N*-(3-sulfopropyl)-ammonium inner salt (F66) as described in Figure 5 for individual cells, which were subsequently normalized to the median value determined in untreated control samples. The number of cells obtained from five independent experiments and involved in the analysis was from left to right: 382, 348, 373, 396, 388, 402 and 393 for Omicron trimer uptake in HEK/ACE2 + TMPRSS2 and 308, 250, 256, 223, 222, 232 and 296 for Omicron trimer uptake in Calu-3. Data points indicated in the figure were obtained from individual cells and plotted along with median values with quartiles. Grey shaded areas show ranges between 0.5 and 1. Asterisks indicate significant differences compared to the control samples (*$P$ < 0.05; one-way ANOVA followed by Tukey's HSD test). See details of statistical analysis in Table S6.

b. All of the effects described above strongly correlated with the extent of structural changes in the membrane and with lipid raft disruption (Figure 1).
c. Cholesterol loading exhibited effects opposite to those of CDs and Veklury® formulations. This is in good agreement with *in vitro* and *in vivo* studies and clinical observations emphasizing the intrinsic connection between SARS-CoV-2, cholesterol and cholesterol-related cardiovascular diseases (Guo et al., 2020; Li et al., 2021; Teixeira et al., 2022; Wang et al., 2021; Williamson, Walker, et al., 2020). It is also suggested by numerous studies that statins, inhibitors of the **HMG-CoA reductase**, and consequent decreases in cholesterol levels could positively correlate with better clinical outcomes in SARS-CoV-2 infection (Daniels et al., 2020; Gupta et al., 2021). Consistently, CDs could serve as an alternative therapeutic approach in the disease through cholesterol extraction, as proposed earlier (Fecchi et al., 2020; Garrido et al., 2020; Palacios-Rápalo et al., 2021; Sorice et al., 2020; Zakany et al., 2022).

The CD and Veklury® concentrations applied in this study, ranging between 0.078 and 20 mM, were chosen to be comparable in magnitude to *in vivo* CD levels in therapeutic applications. In our study, therapeutically relevant CDs and Veklury® formulations did not induce biologically significant changes in cell viabilities even at the largest studied concentrations (Figure S4 and Table S7). The lower end of the concentration range corresponds to the SBECD levels

14765381, 0, Downloaded from https://bpspubs.onlinelibrary.wiley.com/doi/10.1111/bph.16063 by Cochrane Hungary, Wiley Online Library on [03/04/2023]. See the Terms and Conditions (https://onlinelibrary.wiley.com/terms-and-conditions) on Wiley Online Library for rules of use; OA articles are governed by the applicable Creative Commons License

(∼1–2 mM) when applying Veklury®, estimated from pharmacokinetic studies using SBECD (Hoover et al., 2018; Stella & He, 2008). Larger concentrations may also carry medical relevance considering that much higher local concentrations of HPβCD can be observed when it is administered intravenously at doses of 2500 mg·kg$^{-1}$ for the treatment of Niemann–Pick type C disease with relatively good tolerability (Carradori et al., 2020; Davidson et al., 2019; Loftsson & Brewster, 2010; Tanaka et al., 2015; Zakany et al., 2022). REM was typically applied at 100 μM as in most cellular studies (Choy et al., 2020; Wang et al., 2020), which is above those observed after Veklury® treatment (Humeniuk et al., 2020; Sheahan et al., 2017; Warren et al., 2016), whereas CHOL was mostly utilized at 200 μM because it induces increases in membrane cholesterol levels comparable to those observed in patients with hypercholesterolaemia (Somodi et al., 2013; Zakany et al., 2021).

In *in vitro* SARS-CoV-2 research, most model systems apply ACE2-overexpressing HEK cells treated with excessive amounts of spike glycoproteins or viral particles, representing a rather artificial situation of high amounts of interacting receptors and ligands. When examining such conditions in HEK/ACE2 + TMPRSS2 cells, we found relatively modest CD-induced inhibition of ACE2 binding of spike RBDs at high RBD concentrations (Figure 2). However, this effect showed negative correlation with the applied RBD concentration in these cells resulting in much larger reductions at lower RBD levels. Furthermore, larger inhibition was observed in response to CDs in Calu-3 cells with lower receptor expression level in both RBD binding and trimer uptake measurements (Figures 3 and 5). The number of RBD-bound ACE2 was found to be ∼3500 and 500 in HEK/ACE2 + TMPRSS2 and Calu-3 cells, respectively (Note 1 in the supporting information). As few as one to three SARS-CoV-2 virions are assumed to transmit the infection to susceptible persons (Martin & Koelle, 2021) and the number of infectious virions released by infected cells is ∼10/day (Sender et al., 2021; Vaidya et al., 2021). These considerations taken together with the sparse distribution of spike proteins on the surface of intact SARS-CoV-2, making multivalent binding of virions unfavourable (Ke et al., 2020), argue that the number of RBD-bound ACE2 is unlikely to be more than 10 on the surface of cells being infected *in vivo* (Grebennikov et al., 2021). Although we could not model conditions mimicking the pathophysiological situation of infection due to signal-to-noise limitations of the applied methods, extrapolating the trend observed with the high receptor–moderate ligand and low receptor–high ligand models suggests that CD-induced effects and differences between Veklury® P and Veklury® S can in fact be much larger *in vivo*. These findings further emphasize the need for application of more medically relevant experimental systems. Although our study does not provide information about later steps of infection, that is, protease cleavage of spike, membrane fusion, viral RNA replication and virion release, this limitation can be considered as a strength as well because largely neglected initial membrane-coupled events of infection were exclusively examined. Furthermore, our study did not consider CD effects on later stages of SARS-CoV-2 infection *in vivo* such as aggravated immune response and cytokine storm, which eventually lead to severe complications of the disease.

Our findings revealed additional mechanisms of Veklury® actions in the course of SARS-CoV-2 infection. Besides its well-known effect on viral RNA replication due to its remdesivir content, its SBECD component present at high levels in both formulations targets multiple early host cell membrane-related events. Because these initial cholesterol-dependent steps are intrinsic properties of SARS-CoV-2, the multi-level CD action described here can be effective against continuously emerging novel variants as well. In line with this assumption, we found that CDs reduced ACE2 binding and cellular uptake of Delta variant spike RBD and trimers characterized by higher membrane binding affinity (Wang et al., 2022; Yang et al., 2021) (Figure S1D), albeit with slightly lower efficiency (Figures 3 and 5). As opposed to the WT and Delta variants utilizing principally the TMPRSS2-mediated entry pathway, the recently emerged and currently predominant Omicron variant that contains a large number of mutations in the spike resulting in lower efficacy of current vaccines and altered cellular entry mechanisms displays reduced dependence on TMPRSS2 and relies strongly on endocytosis and cathepsin-mediated membrane fusion (Meng et al., 2022; Peacock et al., 2022; Willett et al., 2022). Although we did not compare the extent to which cholesterol depletion reduces the two different cellular entry routes, the fact that the cellular entry of the Omicron variant remained cholesterol-dependent suggests that both the cholesterol-depleting SBECD component of Veklury® formulations and CDs retain their ability to inhibit the initial membrane-coupled events of the viral internalization process.

Although remdesivir formulated as Veklury® was the first approved therapy for severe COVID-19, large-scale randomized clinical trials failed to demonstrate unequivocally its beneficial effects (Ader et al., 2022; Kaka et al., 2022; WHO Solidarity Trial Consortium, 2021). Veklury® P and S were treated equivalently in all of these clinical studies in spite of the doubled SBECD content of the latter and, when documented, Veklury® P was preferentially used due to easier storage. Meta-analytic comparison of the two formulations was carried out only in regard to their renal and hepatic toxicity (Shah et al., 2021) and not based on their efficacy in COVID-19. Given that our results propose the active contribution of SBECD to Veklury® actions, the lack of consideration of different CD levels in the formulations can contribute to its contradictory reputation. Furthermore, our experiments, in light of favourable previous experience with high HPβCD and SBECD doses (Carradori et al., 2020; Davidson et al., 2019; Hoover et al., 2018; Loftsson & Brewster, 2010; Stella & He, 2008; Tanaka et al., 2015), raise the potential benefit of adjuvant CD therapy in early phases of the disease when the symptoms are mainly caused by cellular spreading influenced by the cholesterol-dependent membrane-coupled events. Interestingly, molnupiravir, an antiviral agent recently included in the WHO treatment guidelines in non-severe COVID-19 patients with the highest risk of hospitalization, is also complexed with HPβCD (WHO, 2022). Because lipid rafts generally serve as entry points for a great variety of viruses including other coronaviruses, herpes simplex virus, rotavirus, Ebola or human

14765381, 0, Downloaded from https://bpspubs.onlinelibrary.wiley.com/doi/10.1111/bph.16063 by Cochrane Hungary, Wiley Online Library on [03/04/2023]. See the Terms and Conditions (https://onlinelibrary.wiley.com/terms-and-conditions) on Wiley Online Library for rules of use; OA articles are governed by the applicable Creative Commons License

immunodeficiency virus (Fecchi et al., 2020; Ripa et al., 2021; Sorice et al., 2020; Zakany et al., 2022), CD-induced cholesterol extraction and consequent disruption of these microdomains can represent an unexploited therapeutic approach.

In summary, we showed that Veklury® formulations can actively influence early cholesterol-dependent membrane-coupled entry events of SARS-CoV-2 infection, including reduced RBD binding and cellular trimer uptake, through cholesterol extraction in a remdesivir-independent manner, solely due to their SBECD vehicle. Therefore, at identical remdesivir concentrations, the Veklury® S, having two-fold relative SBECD content, inhibited RBD binding more effectively, calling for its preferential use over the powder format in clinical practice. These results imply that the effects can be even more pronounced at lower RBD concentrations or cell surface ACE2 receptor numbers, thereby potentially increasing the *in vivo* relevance of the hitherto unexploited CD-dependent effects of Veklury®. Despite the fact that the cell tropism, entry mechanism and disease severity are variable in the different variants, the cellular uptake remained basically cholesterol dependent during the continuous evolution of the SARS-CoV-2 virus; thus, the cholesterol-extracting CDs can still be effective against the current and the potential future variants as well. The experimental results may even translate to a potential application of well-tolerable CDs as adjuvants in the therapy of COVID-19.

## AUTHOR CONTRIBUTIONS

**Tamas Kovacs:** Conceptualization (equal); formal analysis (equal); investigation (equal); methodology (equal); visualization (equal); writing—original draft (equal). **Kitti Kurtan:** Formal analysis (equal); investigation (equal). **Zoltan Varga:** Supervision (equal); writing—review and editing (equal). **Peter Nagy:** Formal analysis (equal); methodology (equal); visualization (equal); writing—review and editing (equal). **Gyorgy Panyi:** Funding acquisition (equal); supervision (equal); visualization (equal); writing—review and editing (equal). **Florina Zakany:** Conceptualization (equal); formal analysis (equal); funding acquisition (equal); investigation (equal); methodology (equal); project administration (equal); supervision (equal); visualization (equal); writing—original draft; writing—review and editing (equal).

## ACKNOWLEDGEMENTS

We thank Dr. Mohamed Mahdi (Department of Biochemistry and Molecular Biology, University of Debrecen) and Prof. Attila Toth (Division of Clinical Physiology, Institute of Cardiology, University of Debrecen) for providing the HEK/ACE2 + TMPRSS2 and Calu-3 cells, respectively. We thank the expert technical assistance of Adrienn Bagosi, Rita Utasi-Szabo and Hajnalka Vagone Toldi. This work was supported by the UNKP-22-4-II-DE-69 (F. Z.) New National Excellence Program of the Ministry for Culture and Innovation from the source of the National Research, Development and Innovation Fund; UNKP-21-4-II-DE-138 (F. Z.) and UNKP-21-4-II-DE-137 (T. K.) New National Excellence Program of the Ministry for Innovation and Technology from the source of the National Research, Development and Innovation Fund; the Hungarian National Research, Development and Innovation Office (OTKA FK143400, T. K.; OTKA K138075 and OTKA ANN133421, P. N.; OTKA K132906, Z. V.; and OTKA K143071, G. P.); Ministry of Human Capacities, Hungary (EFOP-3.6.2-16-2017-00006, G. P.); and Ministry of Finance, Hungary (GINOP-2.3.2-15-2016-00015, G. P.).

## CONFLICT OF INTEREST STATEMENT

The authors declare no conflicts of interest.

## DECLARATION OF TRANSPARENCY AND SCIENTIFIC RIGOUR

This Declaration acknowledges that this paper adheres to the principles for transparent reporting and scientific rigour of preclinical research as stated in the *BJP* guidelines for Design & Analysis and as recommended by funding agencies, publishers and other organizations engaged with supporting research.

## DATA AVAILABILITY STATEMENT

The data that support the findings of this study are available from the corresponding author upon reasonable request. Some data may not be made available because of privacy or ethical restrictions.

## ORCID

*Florina Zakany* https://orcid.org/0000-0002-5692-3811

## REFERENCES

Ader, F., Bouscambert-Duchamp, M., Hites, M., Peiffer-Smadja, N., Poissy, J., Belhadi, D., Diallo, A., Lê, M. P., Peytavin, G., Staub, T., Greil, R., Guedj, J., Paiva, J. A., Costagliola, D., Yazdanpanah, Y., Burdet, C., Mentré, F., Egle, A., Greil, R., … Velou, P. (2022). Remdesivir plus standard of care versus standard of care alone for the treatment of patients admitted to hospital with COVID-19 (DisCoVeRy): A phase 3, randomised, controlled, open-label trial. *The Lancet Infectious Diseases*, *22*(2), 209–221. https://doi.org/10.1016/S1473-3099(21)00485-0

Alexander, S. P., Kelly, E., Mathie, A., Peters, J. A., Veale, E. L., Armstrong, J. F., Faccenda, E., Harding, S. D., Pawson, A. J., Southan, C., Buneman, O. P., Cidlowski, J. A., Christopoulos, A., Davenport, A. P., Fabbro, D., Spedding, M., Striessnig, J., Davies, J. A., Ahlers-Dannen, K. E., … Zolghadri, Y. (2021). THE CONCISE GUIDE TO PHARMACOLOGY 2021/22: Introduction and Other Protein Targets. *British Journal of Pharmacology*, *178*(S1), S1–S26. https://doi.org/10.1111/bph.15537

Alexander, S. P., Fabbro, D., Kelly, E., Mathie, A., Peters, J. A., Veale, E. L., Armstrong, J. F., Faccenda, E., Harding, S. D., Pawson, A. J., Southan, C., Davies, J. A., Boison, D., Burns, K. E., Dessauer, C., Gertsch, J., Helsby, N. A., Izzo, A. A., Koesling, D., … Wong, S. S. (2021). THE CONCISE GUIDE TO PHARMACOLOGY 2021/22: Enzymes. *British Journal of Pharmacology*, *178*(S1), S313–S411. https://doi.org/10.1111/bph.15542

Batta, G., Kárpáti, L., Henrique, G. F., Tóth, G., Tarapcsák, S., Kovacs, T., Zakany, F., Mándity, I. M., & Nagy, P. (2021). Statin-boosted cellular uptake and endosomal escape of penetratin due to reduced membrane dipole potential. *British Journal of Pharmacology*, *178*(18), 3667–3681. https://doi.org/10.1111/bph.15509

Bayati, A., Kumar, R., Francis, V., & McPherson, P. S. (2021). SARS-CoV-2 infects cells after viral entry via clathrin-mediated endocytosis. *The Journal of Biological Chemistry*, *296*, 100306. https://doi.org/10.1016/j.jbc.2021.100306

14765381, 0, Downloaded from https://bpspubs.onlinelibrary.wiley.com/doi/10.1111/bph.16063 by Cochrane Hungary, Wiley Online Library on [03/04/2023]. See the Terms and Conditions (https://onlinelibrary.wiley.com/terms-and-conditions) on Wiley Online Library for rules of use; OA articles are governed by the applicable Creative Commons License

Beigel, J. H., Tomashek, K. M., Dodd, L. E., Mehta, A. K., Zingman, B. S., Kalil, A. C., Hohmann, E., Chu, H. Y., Luetkemeyer, A., Kline, S., Lopez de Castilla, D., Finberg, R. W., Dierberg, K., Tapson, V., Hsieh, L., Patterson, T. F., Paredes, R., Sweeney, D. A., Short, W. R., … ACTT-1 Study Group Members. (2020). Remdesivir for the treatment of Covid-19—Final report. *The New England Journal of Medicine*, *383*(19), 1813–1826. https://doi.org/10.1056/NEJMoa2007764

Carradori, D., Chen, H., Werner, B., Shah, A. S., Leonardi, C., Usuelli, M., Mezzenga, R., Platt, F., & Leroux, J. C. (2020). Investigating the mechanism of cyclodextrins in the treatment of Niemann-Pick disease type C using crosslinked 2-hydroxypropyl-β-cyclodextrin. *Small*, *16*(46), e2004735. https://doi.org/10.1002/smll.202004735

Cho, A., Saunders, O. L., Butler, T., Zhang, L., Xu, J., Vela, J. E., Feng, J. Y., Ray, A. S., & Kim, C. U. (2012). Synthesis and antiviral activity of a series of 1′-substituted 4-aza-7,9-dideazaadenosine C-nucleosides. *Bioorganic & Medicinal Chemistry Letters*, *22*(8), 2705–2707. https://doi.org/10.1016/j.bmcl.2012.02.105

Choy, K. T., Wong, A. Y., Kaewpreedee, P., Sia, S. F., Chen, D., Hui, K. P. Y., Chu, D. K. W., Chan, M. C. W., Cheung, P. P. H., Huang, X., Peiris, M., & Yen, H. L. (2020). Remdesivir, lopinavir, emetine, and homoharringtonine inhibit SARS-CoV-2 replication in vitro. *Antiviral Research*, *178*, 104786. https://doi.org/10.1016/j.antiviral.2020.104786

COVID-19 Treatment Guidelines Panel of National Institutes of Health. (2022). *Coronavirus disease 2019 (COVID-19) treatment guidelines*. National Institutes of Health. https://www.covid19treatmentguidelines.nih.gov/

Curtis, M. J., Alexander, S. P. H., Cirino, G., George, C. H., Kendall, D. A., Insel, P. A., Izzo, A. A., Ji, Y., Panettieri, R. A., Patel, H. H., Sobey, C. G., Stanford, S. C., Stanley, P., Stefanska, B., Stephens, G. J., Teixeira, M. M., Vergnolle, N., & Ahluwalia, A. (2022). Planning experiments: Updated guidance on experimental design and analysis and their reporting III. *British Journal of Pharmacology*, *179*, 3907–3913. https://doi.org/10.1111/bph.15868

Daniels, L. B., Sitapati, A. M., Zhang, J., Zou, J., Bui, Q. M., Ren, J., Longhurst, C. A., Criqui, M. H., & Messer, K. (2020). Relation of statin use prior to admission to severity and recovery among COVID-19 inpatients. *The American Journal of Cardiology*, *136*, 149–155. https://doi.org/10.1016/j.amjcard.2020.09.012

Davidson, C. D., Fishman, Y. I., Puskás, I., Szemán, J., Sohajda, T., McCauliff, L. A., Sikora, J., Storch, J., Vanier, M. T., Szente, L., Walkley, S. U., & Dobrenis, K. (2016). Efficacy and ototoxicity of different cyclodextrins in Niemann–Pick C disease. *Annals of Clinical Translational Neurology*, *3*(5), 366–380. https://doi.org/10.1002/acn3.306

Davidson, J., Molitor, E., Moores, S., Gale, S. E., Subramanian, K., Jiang, X., Sidhu, R., Kell, P., Zhang, J., Fujiwara, H., Davidson, C., Helquist, P., Melancon, B. J., Grigalunas, M., Liu, G., Salahi, F., Wiest, O., Xu, X., Porter, F. D., … Ory, D. S. (2019). 2-Hydroxypropyl-β-cyclodextrin is the active component in a triple combination formulation for treatment of Niemann-Pick C1 disease. *Biochimica et Biophysica Acta - Molecular and Cell Biology of Lipids*, *1864*(10), 1545–1561. https://doi.org/10.1016/j.bbalip.2019.04.011

de Wit, E., Feldmann, F., Cronin, J., Jordan, R., Okumura, A., Thomas, T., Scott, D., Cihlar, T., & Feldmann, H. (2020). Prophylactic and therapeutic remdesivir (GS-5734) treatment in the rhesus macaque model of MERS-CoV infection. *Proceedings of the National Academy of Sciences of the United States of America*, *117*(12), 6771–6776. https://doi.org/10.1073/pnas.1922083117

Fecchi, K., Anticoli, S., Peruzzu, D., Iessi, E., Gagliardi, M. C., Matarrese, P., & Ruggieri, A. (2020). Coronavirus interplay with lipid rafts and autophagy unveils promising therapeutic targets. *Frontiers in Microbiology*, *11*, 1821. https://doi.org/10.3389/fmicb.2020.01821

Garrido, P. F., Calvelo, M., Blanco-González, A., Veleiro, U., Suárez, F., Conde, D., Cabezón, A., Piñeiro, Á., & Garcia-Fandino, R. (2020). The Lord of the NanoRings: Cyclodextrins and the battle against SARS-CoV-2. *International Journal of Pharmaceutics*, *588*, 119689. https://doi.org/10.1016/j.ijpharm.2020.119689

Gilead Sciences, Inc. (2022). Veklury® prescribing information. https://www.gilead.com/-/media/files/pdfs/medicines/covid-19/veklury/veklury_pi.pdf

Gottlieb, R. L., Vaca, C. E., Paredes, R., Mera, J., Webb, B. J., Perez, G., Oguchi, G., Ryan, P., Nielsen, B. U., Brown, M., Hidalgo, A., Sachdeva, Y., Mittal, S., Osiyemi, O., Skarbinski, J., Juneja, K., Hyland, R. H., Osinusi, A., Chen, S., … GS-US-540-9012 (PINETREE) Investigators. (2022). Early remdesivir to prevent progression to severe Covid-19 in outpatients. *The New England Journal of Medicine*, *386*(4), 305–315. https://doi.org/10.1056/NEJMoa2116846

Grebennikov, D., Kholodareva, E., Sazonov, I., Karsonova, A., Meyerhans, A., & Bocharov, G. (2021). Intracellular life cycle kinetics of SARS-CoV-2 predicted using mathematical modelling. *Viruses*, *13*(9), 1735. https://doi.org/10.3390/v13091735

Guo, T., Fan, Y., Chen, M., Wu, X., Zhang, L., He, T., Wang, H., Wan, J., Wang, X., & Lu, Z. (2020). Cardiovascular implications of fatal outcomes of patients with coronavirus disease 2019 (COVID-19). *JAMA Cardiology*, *5*(7), 811–818. https://doi.org/10.1001/jamacardio.2020.1017

Gupta, A., Madhavan, M. V., Poterucha, T. J., DeFilippis, E. M., Hennessey, J. A., Redfors, B., Eckhardt, C., Bikdeli, B., Platt, J., Nalbandian, A., Elias, P., Cummings, M. J., Nouri, S. N., Lawlor, M., Ranard, L. S., Li, J., Boyle, C., Givens, R., Brodie, D., … Parikh, S. A. (2021). Association between antecedent statin use and decreased mortality in hospitalized patients with COVID-19. *Nature Communications*, *12*(1), 1325. https://doi.org/10.1038/s41467-021-21553-1

Ho, W. S., Zhang, R., Tan, Y. L., & Chai, C. L. L. (2022). COVID-19 and the promise of small molecule therapeutics: Are there lessons to be learnt? *Pharmacological Research*, *179*, 106201. https://doi.org/10.1016/j.phrs.2022.106201

Hoffmann, M., Kleine-Weber, H., Schroeder, S., Krüger, N., Herrler, T., Erichsen, S., Schiergens, T. S., Herrler, G., Wu, N. H., Nitsche, A., Müller, M. A., Drosten, C., & Pöhlmann, S. (2020). SARS-CoV-2 cell entry depends on ACE2 and TMPRSS2 and is blocked by a clinically proven protease inhibitor. *Cell*, *181*(2), 271–280.e8. https://doi.org/10.1016/j.cell.2020.02.052

Hoover, R. K., Alcorn, H. Jr., Lawrence, L., Paulson, S. K., Quintas, M., Luke, D. R., & Cammarata, S. K. (2018). Clinical pharmacokinetics of sulfobutylether-β-cyclodextrin in patients with varying degrees of renal impairment. *Journal of Clinical Pharmacology*, *58*(6), 814–822. https://doi.org/10.1002/jcph.1077

Humeniuk, R., Mathias, A., Cao, H., Osinusi, A., Shen, G., Chng, E., Ling, J., Vu, A., & German, P. (2020). Safety, tolerability, and pharmacokinetics of remdesivir, an antiviral for treatment of COVID-19, in healthy subjects. *Clinical and Translational Science*, *13*(5), 896–906. https://doi.org/10.1111/cts.12840

Jackson, C. B., Farzan, M., Chen, B., & Choe, H. (2022). Mechanisms of SARS-CoV-2 entry into cells. *Nature Reviews. Molecular Cell Biology*, *23*(1), 3–20. https://doi.org/10.1038/s41580-021-00418-x

Kaka, A. S., MacDonald, R., Linskens, E. J., Langsetmo, L., Vela, K., Duan-Porter, W., & Wilt, T. J. (2022). Major update 2: Remdesivir for adults with COVID-19: A living systematic review and meta-analysis for the American College of Physicians practice points. *Annals of Internal Medicine*, *175*, 701–709. https://doi.org/10.7326/M21-4784

Ke, Z., Oton, J., Qu, K., Cortese, M., Zila, V., McKeane, L., Nakane, T., Zivanov, J., Neufeldt, C. J., Cerikan, B., Lu, J. M., Peukes, J., Xiong, X., Kräusslich, H. G., Scheres, S. H. W., Bartenschlager, R., & Briggs, J. A. G. (2020). Structures and distributions of SARS-CoV-2 spike proteins on intact virions. *Nature*, *588*(7838), 498–502. https://doi.org/10.1038/s41586-020-2665-2

Kovacs, T., Batta, G., Zakany, F., Szollosi, J., & Nagy, P. (2017). The dipole potential correlates with lipid raft markers in the plasma membrane of living cells. *Journal of Lipid Research*, *58*(8), 1681–1691. https://doi.org/10.1194/jlr.M077339

14765381, 0, Downloaded from https://bpspubs.onlinelibrary.wiley.com/doi/10.1111/bph.16063 by Cochrane Hungary, Wiley Online Library on [03/04/2023]. See the Terms and Conditions (https://onlinelibrary.wiley.com/terms-and-conditions) on Wiley Online Library for rules of use; OA articles are governed by the applicable Creative Commons License

Kovacs, T., Nagy, P., Panyi, G., Szente, L., Varga, Z., & Zakany, F. (2022). Cyclodextrins: Only pharmaceutical excipients or full-fledged drug candidates? *Pharmaceutics*, *14*(12), 2559. https://doi.org/10.3390/pharmaceutics14122559

Kovacs, T., Sohajda, T., Szente, L., Nagy, P., Panyi, G., Varga, Z., & Zakany, F. (2021). Cyclodextrins exert a ligand-like current inhibitory effect on the $K_V1.3$ ion channel independent of membrane cholesterol extraction. *Frontiers in Molecular Biosciences*, *8*, 735357. https://doi.org/10.3389/fmolb.2021.735357

Li, X., Zhu, W., Fan, M., Zhang, J., Peng, Y., Huang, F., Wang, N., He, L., Zhang, L., Holmdahl, R., Meng, L., & Lu, S. (2021). Dependence of SARS-CoV-2 infection on cholesterol-rich lipid raft and endosomal acidification. *Computational and Structural Biotechnology Journal*, *19*, 1933–1943. https://doi.org/10.1016/j.csbj.2021.04.001

Loftsson, T., & Brewster, M. E. (2010). Pharmaceutical applications of cyclodextrins: Basic science and product development. *The Journal of Pharmacy and Pharmacology*, *62*(11), 1607–1621. https://doi.org/10.1111/j.2042-7158.2010.01030.x

Malek, R. J., Bill, C. A., & Vines, C. M. (2021). Clinical drug therapies and biologicals currently used or in clinical trial to treat COVID-19. *Biomedicine & Pharmacotherapy*, *144*, 112276. https://doi.org/10.1016/j.biopha.2021.112276

Martin, M. A., & Koelle, K. (2021). Comment on "Genomic epidemiology of superspreading events in Austria reveals mutational dynamics and transmission properties of SARS-CoV-2". *Science Translational Medicine*, *13*(617), eabh1803. https://doi.org/10.1126/scitranslmed.abh1803

Meng, B., Abdullahi, A., Ferreira, I., Goonawardane, N., Saito, A., Kimura, I., Yamasoba, D., Gerber, P. P., Fatihi, S., Rathore, S., Zepeda, S. K., Papa, G., Kemp, S. A., Ikeda, T., Toyoda, M., Tan, T. S., Kuramochi, J., Mitsunaga, S., Ueno, T., … Gupta, R. K. (2022). Altered TMPRSS2 usage by SARS-CoV-2 Omicron impacts infectivity and fusogenicity. *Nature*, *603*(7902), 706–714. https://doi.org/10.1038/s41586-022-04474-x

Ou, X., Liu, Y., Lei, X., Li, P., Mi, D., Ren, L., Guo, L., Guo, R., Chen, T., Hu, J., Xiang, Z., Mu, Z., Chen, X., Chen, J., Hu, K., Jin, Q., Wang, J., & Qian, Z. (2020). Characterization of spike glycoprotein of SARS-CoV-2 on virus entry and its immune cross-reactivity with SARS-CoV. *Nature Communications*, *11*(1), 1620. https://doi.org/10.1038/s41467-020-15562-9

Palacios-Rápalo, S. N., de Jesús-González, L. A., Cordero-Rivera, C. D., Farfan-Morales, C. N., Osuna-Ramos, J. F., Martínez-Mier, G., Quistián-Galván, J., Muñoz-Pérez, A., Bernal-Dolores, V., del Ángel, R. M., & Reyes-Ruiz, J. M. (2021). Cholesterol-rich lipid rafts as platforms for SARS-CoV-2 entry. *Frontiers in Immunology*, *12*, 796855. https://doi.org/10.3389/fimmu.2021.796855

Peacock, T. P., Brown, J. C., Zhou, J., Thakur, N., Sukhova, K., Newman, J., Kugathasan, R., Yan, A. W. C., Furnon, W., De Lorenzo, G., Cowton, V. M., Reuss, D., Moshe, M., Quantrill, J. L., Platt, O. K., Kaforou, M., Patel, A. H., Palmarini, M., Bailey, D., & Barclay, W. S. (2022). The altered entry pathway and antigenic distance of the SARS-CoV-2 Omicron variant map to separate domains of spike protein. *bioRxiv*, 2021.12.31.474653. https://doi.org/10.1101/2021.12.31.474653

Planas, D., Veyer, D., Baidaliuk, A., Staropoli, I., Guivel-Benhassine, F., Rajah, M. M., Planchais, C., Porrot, F., Robillard, N., Puech, J., Prot, M., Gallais, F., Gantner, P., Velay, A., le Guen, J., Kassis-Chikhani, N., Edriss, D., Belec, L., Seve, A., … Schwartz, O. (2021). Reduced sensitivity of SARS-CoV-2 variant Delta to antibody neutralization. *Nature*, *596*(7871), 276–280. https://doi.org/10.1038/s41586-021-03777-9

Pruijssers, A. J., George, A. S., Schäfer, A., Leist, S. R., Gralinksi, L. E., Dinnon, K. H. 3rd, Yount, B. L., Agostini, M. L., Stevens, L. J., Chappell, J. D., Lu, X., Hughes, T. M., Gully, K., Martinez, D. R., Brown, A. J., Graham, R. L., Perry, J. K., du Pont, V., Pitts, J., … Sheahan, T. P. (2020). Remdesivir inhibits SARS-CoV-2 in human lung cells and chimeric SARS-CoV expressing the SARS-CoV-2 RNA polymerase in mice. *Cell Reports*, *32*(3), 107940. https://doi.org/10.1016/j.celrep.2020.107940

Ripa, I., Andreu, S., Lopez-Guerrero, J. A., & Bello-Morales, R. (2021). Membrane rafts: Portals for viral entry. *Frontiers in Microbiology*, *12*, 631274. https://doi.org/10.3389/fmicb.2021.631274

Sanders, J. M., Monogue, M. L., Jodlowski, T. Z., & Cutrell, J. B. (2020). Pharmacologic treatments for coronavirus disease 2019 (COVID-19): A review. *Jama*, *323*(18), 1824–1836. https://doi.org/10.1001/jama.2020.6019

Sender, R., Bar-On, Y. M., Gleizer, S., Bernshtein, B., Flamholz, A., Phillips, R., & Milo, R. (2021). The total number and mass of SARS-CoV-2 virions. *Proceedings of the National Academy of Sciences of the United States of America*, *118*(25), e2024815118. https://doi.org/10.1073/pnas.2024815118

Sezgin, E., Levental, I., Mayor, S., & Eggeling, C. (2017). The mystery of membrane organization: Composition, regulation and roles of lipid rafts. *Nature Reviews. Molecular Cell Biology*, *18*(6), 361–374. https://doi.org/10.1038/nrm.2017.16

Shah, S., Ackley, T. W., & Topal, J. E. (2021). Renal and hepatic toxicity analysis of remdesivir formulations: Does what is on the inside really count? *Antimicrobial Agents and Chemotherapy*, *65*(10), e0104521. https://doi.org/10.1128/AAC.01045-21

Sheahan, T. P., Sims, A. C., Graham, R. L., Menachery, V. D., Gralinski, L. E., Case, J. B., Leist, S. R., Pyrc, K., Feng, J. Y., Trantcheva, I., Bannister, R., Park, Y., Babusis, D., Clarke, M. O., Mackman, R. L., Spahn, J. E., Palmiotti, C. A., Siegel, D., Ray, A. S., … Baric, R. S. (2017). Broad-spectrum antiviral GS-5734 inhibits both epidemic and zoonotic coronaviruses. *Science Translational Medicine*, *9*(396), eaal3653. https://doi.org/10.1126/scitranslmed.aal3653

Sheahan, T. P., Sims, A. C., Leist, S. R., Schäfer, A., Won, J., Brown, A. J., Montgomery, S. A., Hogg, A., Babusis, D., Clarke, M. O., Spahn, J. E., Bauer, L., Sellers, S., Porter, D., Feng, J. Y., Cihlar, T., Jordan, R., Denison, M. R., & Baric, R. S. (2020). Comparative therapeutic efficacy of remdesivir and combination lopinavir, ritonavir, and interferon beta against MERS-CoV. *Nature Communications*, *11*(1), 222. https://doi.org/10.1038/s41467-019-13940-6

Siegel, D., Hui, H. C., Doerffler, E., Clarke, M. O., Chun, K., Zhang, L., Neville, S., Carra, E., Lew, W., Ross, B., Wang, Q., Wolfe, L., Jordan, R., Soloveva, V., Knox, J., Perry, J., Perron, M., Stray, K. M., Barauskas, O., … Mackman, R. L. (2017). Discovery and synthesis of a phosphoramidate prodrug of a pyrrolo[2,1-*f*][triazin-4-amino] adenine *C*-nucleoside (GS-5734) for the treatment of Ebola and emerging viruses. *Journal of Medicinal Chemistry*, *60*(5), 1648–1661. https://doi.org/10.1021/acs.jmedchem.6b01594

Somodi, S., Balajthy, A., Szilágyi, O., Pethő, Z., Harangi, M., Paragh, G., Panyi, G., & Hajdu, P. (2013). Analysis of the $K^+$ current in human $CD4^+$ T lymphocytes in hypercholesterolemic state. *Cellular Immunology*, *281*(1), 20–26. https://doi.org/10.1016/j.cellimm.2013.01.004

Sorice, M., Misasi, R., Riitano, G., Manganelli, V., Martellucci, S., Longo, A., Garofalo, T., & Mattei, V. (2020). Targeting lipid rafts as a strategy against coronavirus. *Frontiers in Cell and Development Biology*, *8*, 618296. https://doi.org/10.3389/fcell.2020.618296

Spinner, C. D., Gottlieb, R. L., Criner, G. J., Arribas López, J. R., Cattelan, A. M., Soriano Viladomiu, A., Ogbuagu, O., Malhotra, P., Mullane, K. M., Castagna, A., Chai, L. Y. A., Roestenberg, M., Tsang, O. T. Y., Bernasconi, E., le Turnier, P., Chang, S. C., SenGupta, D., Hyland, R. H., Osinusi, A. O., … GS-US-540-5774 Investigators. (2020). Effect of remdesivir vs standard care on clinical status at 11 days in patients with moderate COVID-19: A randomized clinical trial. *Jama*, *324*(11), 1048–1057. https://doi.org/10.1001/jama.2020.16349

Stella, V. J., & He, Q. (2008). Cyclodextrins. *Toxicologic Pathology*, *36*(1), 30–42. https://doi.org/10.1177/0192623307310945

Szente, L., Puskás, I., Sohajda, T., Varga, E., Vass, P., Nagy, Z. K., Farkas, A., Várnai, B., Béni, S., & Hazai, E. (2021). Sulfobutylether-beta-cyclodextrin-enabled antiviral remdesivir: Characterization of electrospun- and lyophilized formulations. *Carbohydrate Polymers*, *264*, 118011. https://doi.org/10.1016/j.carbpol.2021.118011

14765381, 0, Downloaded from https://bpspubs.onlinelibrary.wiley.com/doi/10.1111/bph.16063 by Cochrane Hungary, Wiley Online Library on [03/04/2023]. See the Terms and Conditions (https://onlinelibrary.wiley.com/terms-and-conditions) on Wiley Online Library for rules of use; OA articles are governed by the applicable Creative Commons License

Szente, L., Singhal, A., Domokos, A., & Song, B. (2018). Cyclodextrins: Assessing the impact of cavity size, occupancy, and substitutions on cytotoxicity and cholesterol homeostasis. *Molecules*, *23*(5), 1228. https://doi.org/10.3390/molecules23051228

Tanaka, Y., Yamada, Y., Ishitsuka, Y., Matsuo, M., Shiraishi, K., Wada, K., Uchio, Y., Kondo, Y., Takeo, T., Nakagata, N., Higashi, T., Motoyama, K., Arima, H., Mochinaga, S., Higaki, K., Ohno, K., & Irie, T. (2015). Efficacy of 2-hydroxypropyl-β-cyclodextrin in Niemann–Pick disease type C model mice and its pharmacokinetic analysis in a patient with the disease. *Biological & Pharmaceutical Bulletin*, *38*(6), 844–851. https://doi.org/10.1248/bpb.b14-00726

Teixeira, L., Temerozo, J. R., Pereira-Dutra, F. S., Ferreira, A. C., Mattos, M., Gonçalves, B. S., Sacramento, C. Q., Palhinha, L., Cunha-Fernandes, T., Dias, S. S. G., Soares, V. C., Barreto, E. A., Cesar-Silva, D., Fintelman-Rodrigues, N., Pão, C. R. R., de Freitas, C. S., Reis, P. A., Hottz, E. D., Bozza, F. A., … Bozza, P. T. (2022). Simvastatin downregulates the SARS-CoV-2-induced inflammatory response and impairs viral infection through disruption of lipid rafts. *Frontiers in Immunology*, *13*, 820131. https://doi.org/10.3389/fimmu.2022.820131

Tregoning, J. S., Flight, K. E., Higham, S. L., Wang, Z., & Pierce, B. F. (2021). Progress of the COVID-19 vaccine effort: Viruses, vaccines and variants versus efficacy, effectiveness and escape. *Nature Reviews. Immunology*, *21*(10), 626–636. https://doi.org/10.1038/s41577-021-00592-1

Vaidya, N. K., Bloomquist, A., & Perelson, A. S. (2021). Modeling within-host dynamics of SARS-CoV-2 infection: A case study in ferrets. *Viruses*, *13*(8), 1635. https://doi.org/10.3390/v13081635

Wang, H., Yuan, Z., Pavel, M. A., Jablonski, S. M., Jablonski, J., Hobson, R., Valente, S., Reddy, C. B., & Hansen, S. B. (2021). The role of high cholesterol in age-related COVID19 lethality. *bioRxiv*, 2020.05.09.086249. https://doi.org/10.1101/2020.05.09.086249

Wang, M., Cao, R., Zhang, L., Yang, X., Liu, J., Xu, M., Shi, Z., Hu, Z., Zhong, W., & Xiao, G. (2020). Remdesivir and chloroquine effectively inhibit the recently emerged novel coronavirus (2019-nCoV) in vitro. *Cell Research*, *30*(3), 269–271. https://doi.org/10.1038/s41422-020-0282-0

Wang, Y., Liu, C., Zhang, C., Wang, Y., Hong, Q., Xu, S., Li, Z., Yang, Y., Huang, Z., & Cong, Y. (2022). Structural basis for SARS-CoV-2 Delta variant recognition of ACE2 receptor and broadly neutralizing antibodies. *Nature Communications*, *13*(1), 871. https://doi.org/10.1038/s41467-022-28528-w

Warren, T. K., Jordan, R., Lo, M. K., Ray, A. S., Mackman, R. L., Soloveva, V., Siegel, D., Perron, M., Bannister, R., Hui, H. C., Larson, N., Strickley, R., Wells, J., Stuthman, K. S., van Tongeren, S. A., Garza, N. L., Donnelly, G., Shurtleff, A. C., Retterer, C. J., … Bavari, S. (2016). Therapeutic efficacy of the small molecule GS-5734 against Ebola virus in rhesus monkeys. *Nature*, *531*(7594), 381–385. https://doi.org/10.1038/nature17180

WHO Solidarity Trial Consortium. (2021). Repurposed antiviral drugs for Covid-19—Interim WHO Solidarity Trial results. *The New England Journal of Medicine*, *384*(6), 497–511. https://doi.org/10.1056/NEJMoa2023184

Willett, B. J., Grove, J., MacLean, O. A., Wilkie, C., de Lorenzo, G., Furnon, W., Cantoni, D., Scott, S., Logan, N., Ashraf, S., Manali, M., Szemiel, A., Cowton, V., Vink, E., Harvey, W. T., Davis, C., Asamaphan, P., Smollett, K., Tong, L., … Thomson, E. C. (2022). SARS-CoV-2 Omicron is an immune escape variant with an altered cell entry pathway. *Nature Microbiology*, *7*(8), 1161–1179. https://doi.org/10.1038/s41564-022-01143-7

Williamson, B. N., Feldmann, F., Schwarz, B., Meade-White, K., Porter, D. P., Schulz, J., van Doremalen, N., Leighton, I., Yinda, C. K., Pérez-Pérez, L., Okumura, A., Lovaglio, J., Hanley, P. W., Saturday, G., Bosio, C. M., Anzick, S., Barbian, K., Cihlar, T., Martens, C., … de Wit, E. (2020). Clinical benefit of remdesivir in rhesus macaques infected with SARS-CoV-2. *Nature*, *585*(7824), 273–276. https://doi.org/10.1038/s41586-020-2423-5

Williamson, E. J., Walker, A. J., Bhaskaran, K., Bacon, S., Bates, C., Morton, C. E., Curtis, H. J., Mehrkar, A., Evans, D., Inglesby, P., Cockburn, J., McDonald, H. I., MacKenna, B., Tomlinson, L., Douglas, I. J., Rentsch, C. T., Mathur, R., Wong, A. Y. S., Grieve, R., … Goldacre, B. (2020). Factors associated with COVID-19-related death using OpenSAFELY. *Nature*, *584*(7821), 430–436. https://doi.org/10.1038/s41586-020-2521-4

World Health Organization. (2022). Therapeutics and COVID-19: Living guideline. https://www.who.int/publications/i/item/WHO-2019-nCoV-therapeutics-2022.3

Yang, T.-J., Yu, P.-Y., Chang, Y.-C., Chang, N.-E., Tsai, Y.-X., Liang, K.-H., Draczkowski, P., Lin, B., Wang, Y. S., Chien, Y. C., Khoo, K. H., & Hsu, S.-T. D. (2021). Structure-activity relationships of B.1.617 and other SARS-CoV-2 spike variants. *bioRxiv*, 2021.09.12.459978. https://doi.org/10.1101/2021.09.12.459978

Zakany, F., Kovacs, T., Panyi, G., & Varga, Z. (2020). Direct and indirect cholesterol effects on membrane proteins with special focus on potassium channels. *Biochimica et Biophysica Acta - Molecular and Cell Biology of Lipids*, *1865*(8), 158706. https://doi.org/10.1016/j.bbalip.2020.158706

Zakany, F., Kovacs, T., Szente, L., & Varga, Z. (2022). Chapter 34—Cyclodextrins as promising therapeutics against cholesterol overload. In A. N. Bukiya & A. M. Dopico (Eds.), *Cholesterol* (pp. 927–967). Academic Press. https://doi.org/10.1016/B978-0-323-85857-1.00028-6

Zakany, F., Szabo, M., Batta, G., Kárpáti, L., Mándity, I. M., Fülöp, P., Varga, Z., Panyi, G., Nagy, P., & Kovacs, T. (2021). An ω-3, but not an ω-6 polyunsaturated fatty acid decreases membrane dipole potential and stimulates endo-lysosomal escape of penetratin. *Frontiers in Cell and Development Biology*, *9*, 647300. https://doi.org/10.3389/fcell.2021.647300

Zhou, P., Yang, X. L., Wang, X. G., Hu, B., Zhang, L., Zhang, W., Si, H. R., Zhu, Y., Li, B., Huang, C. L., Chen, H. D., Chen, J., Luo, Y., Guo, H., Jiang, R. D., Liu, M. Q., Chen, Y., Shen, X. R., Wang, X., … Shi, Z. L. (2020). A pneumonia outbreak associated with a new coronavirus of probable bat origin. *Nature*, *579*(7798), 270–273. https://doi.org/10.1038/s41586-020-2012-7

Zhu, N., Zhang, D., Wang, W., Li, X., Yang, B., Song, J., Zhao, X., Huang, B., Shi, W., Lu, R., Niu, P., Zhan, F., Ma, X., Wang, D., Xu, W., Wu, G., Gao, G. F., Tan, W., & China Novel Coronavirus Investigating and Research Team. (2020). A novel coronavirus from patients with pneumonia in China, 2019. *The New England Journal of Medicine*, *382*(8), 727–733. https://doi.org/10.1056/NEJMoa2001017

Zidovetzki, R., & Levitan, I. (2007). Use of cyclodextrins to manipulate plasma membrane cholesterol content: Evidence, misconceptions and control strategies. *Biochimica et Biophysica Acta*, *1768*(6), 1311–1324. https://doi.org/10.1016/j.bbamem.2007.03.026

## SUPPORTING INFORMATION

Additional supporting information can be found online in the Supporting Information section at the end of this article.

**How to cite this article:** Kovacs, T., Kurtan, K., Varga, Z., Nagy, P., Panyi, G., & Zakany, F. (2023). Veklury® (remdesivir) formulations inhibit initial membrane-coupled events of SARS-CoV-2 infection due to their sulfobutylether-β-cyclodextrin content. *British Journal of Pharmacology*, 1–21. https://doi.org/10.1111/bph.16063

14765381, 0, Downloaded from https://bpspubs.onlinelibrary.wiley.com/doi/10.1111/bph.16063 by Cochrane Hungary, Wiley Online Library on [03/04/2023]. See the Terms and Conditions (https://onlinelibrary.wiley.com/terms-and-conditions) on Wiley Online Library for rules of use; OA articles are governed by the applicable Creative Commons License